

SPACE-TIME ISOGEOMETRIC ANALYSIS OF PARABOLIC EVOLUTION EQUATIONS

Ulrich Langer¹, Stephen E. Moore¹ and Martin Neumüller²

¹ Johann Radon Institute for Computational and Applied Mathematics,
Austrian Academy of Sciences, Altenberger Str. 69, 4040 Linz, Austria.

² Institute of Computational Mathematics, Johannes Kepler University,
Altenberger Str. 69, 4040 Linz, Austria.

(ulrich.langer, stephen.moore)@ricam.oeaw.ac.at,
neumueller@numa.uni-linz.ac.at

Abstract. We present and analyze a new stable space-time Isogeometric Analysis (IgA) method for the numerical solution of parabolic evolution equations in fixed and moving spatial computational domains. The discrete bilinear form is elliptic on the IgA space with respect to a discrete energy norm. This property together with a corresponding boundedness property, consistency and approximation results for the IgA spaces yields an a priori discretization error estimate with respect to the discrete norm. The theoretical results are confirmed by several numerical experiments with low- and high-order IgA spaces.

Key words: parabolic initial-boundary value problems, space-time isogeometric analysis, fixed and moving spatial computational domains, a priori discretization error estimates

1 Introduction

Let us consider the parabolic initial-boundary value problem: find $u : \overline{Q} \rightarrow \mathbb{R}$ such that

$$\begin{aligned} \partial_t u(x, t) - \Delta u(x, t) &= f(x, t) & \text{for } (x, t) \in Q := \Omega \times (0, T), \\ u(x, t) &= 0 & \text{for } (x, t) \in \Sigma := \partial\Omega \times (0, T), \\ u(x, 0) &= u_0(x) & \text{for } x \in \overline{\Omega}, \end{aligned} \quad (1.1)$$

as the typical model problem for a linear parabolic evolution equation posed in the space-time cylinder $\overline{Q} = \overline{\Omega} \times [0, T]$, where ∂_t denotes the partial time derivative, Δ is the Laplace operator, f is a given source function, u_0 are the given initial data, T is the final time, and $\Omega \subset \mathbb{R}^d$ ($d = 1, 2, 3$) denotes the spatial computational domain with the boundary $\partial\Omega$. For the time being, we assume that the domain Ω is fixed, bounded

and Lipschitz. In many practical, in particular, industrial applications, the domain Ω , that is also called physical domain, is usually generated by some CAD system, i.e., it can be represented by a single patch or multiple patches which are images of the parameter domain $(0, 1)^d$ by spline or NURBS maps.

The standard discretization methods in time and space are based on time-stepping methods combined with some spatial discretization technique like the Finite Element Method (FEM) [26,52,31]. The vertical method of lines discretizes first in time and then in space [52], whereas in the horizontal method of lines, also called Rothe's method, the discretization starts with respect to (wrt) the time variable [31]. The later method has some advantages wrt the development of adaptive techniques. However, in both approaches, the development of really efficient adaptive techniques suffers from the separation of the time and the space discretizations. Moreover, this separation is even more problematic in parallel computing. The curse of sequentiality of time affects the construction of efficient parallel method and their implementation of massively parallel computers with several thousands or even hundreds of thousands of cores in a very bad way.

The simplest ideas for space-time solvers are based on time-parallel integration techniques for ordinary differential equations that have a long history, see [13] for a comprehensive presentation of this history. The most popular parallel time integration method is the parareal method that was introduced by Lions, Maday and Turinici in [35]. Time-parallel multigrid methods have also a long history. In 1984, Hackbusch proposed the so-called parabolic multigrid method that allows a simultaneous execution on a set of successive time steps [17]. Lubich and Ostermann [36] introduced parallel multigrid waveform relaxation methods for parabolic problems. A comprehensive presentation of these methods and a survey of the references until 1993 can be found in the monograph [56]. Vandewalle and Horton investigate the convergence behavior of these time-parallel multigrid methods by means of Fourier mode analysis [19]. Deshpande et al. provided a rigorous analysis of time domain parallelism [11]. Very recently, Gander and Neumüller have also used the Fourier analysis to construct perfectly scaling parallel space-time multigrid methods for solving initial value problems for ordinary differential equations [15] and initial-boundary value problems for parabolic PDEs [14]. In these two papers, the authors construct stable high-order dG discretizations in time slices. In [39] this technique is used to solve the arising linear system of a space-time dG discretization, which is also stable in the case of the decomposition

of the space-time cylinder into 4d simplices (pentatops) for 3d spatial computational domains. This idea opens great opportunities for flexible discretizations, adaptivity and the treatment of changing spatial domains in time [40,41,39,25]. We also refer to [55,1,6,49,50,51,48,37,8,34] where different space-time techniques have been developed. One class of special space-time methods, that is very relevant to single-patch space-time IgA, which we are going to consider in this paper, is the multiharmonic or harmonic balanced FEM that was first used for solving non-linear, time-harmonic eddy current problems by electrical engineers, see, e.g., [58]. Lately the multiharmonic FEM has been applied to parabolic and eddy current time-periodic boundary value problems as well as to the corresponding optimal control problems, see [4,27,28,32]. Babuska and Janik already developed $h - p$ versions of the finite element method in space with p and $h - p$ approximations in time for parabolic initial boundary value problems in the papers [2] and [3], respectively. In [44], Schwab and Stevenson have recently developed and analyzed space-time adaptive wavelet methods for parabolic evolution problems, see also [9]. Similarly, Mollet proved uniform stability of an abstract Petrov-Galerkin discretizations of boundedly invertible operators and applied this result to space-time discretizations of linear parabolic problems [38]. Very recently Urban and Patera have proved error bounds for reduced basis approximation to linear parabolic problems [54], whereas Steinbach has investigated conform space-time finite element approximations to parabolic problems [46]. We here also mention the papers by Olshanskii and Reusken who have developed Eulerian space-time finite element method for diffusion problems on evolving surfaces [43,42]. Our approach uses special time-upwind test functions which are motivated by a space-time streamline diffusion method [18,21,22,23] and by a similar approach used in [5].

The increasing interest in highly time-parallel space-time methods is certainly connected with the fact that parallel computers have rapidly developed with respect to number of cores, computation speed, memory, availability etc, but also with the complexity of the problems the people want to solve. In particular, the optimization of products and processes on the basis of computer simulations of the underlying transient processes (PDE constrains) foster the development of space-time methods since the optimality system is basically nothing but a system of primal and adjoint PDEs which are coupled forward and backward in time, see, e.g., [53]. To the best of our knowledge, we are not aware of any paper on space-time IgA for evolution equations.

In this paper, we present a stable discrete space-time variational formulation for the parabolic initial-boundary value problems of the form (1.1) in the sense that the discrete bilinear form $a_h(\cdot, \cdot) : V_{0h} \times V_{0h} \rightarrow \mathbb{R}$ is elliptic on the IgA space V_{0h} wrt a special discrete norm $\|\cdot\|_h$. For simplicity, we consider the single-patch case where the space-time cylinder Q , that is called physical domain, can be represented by one smooth, uniformly regular spline or NURBS map Φ of the parameter domain $\widehat{Q} = (0, 1)^{d+1}$. In IgA, that was introduced by Hughes, Cottrell and Bazilevs in 2005 [20], we use the same basis functions for both representing the approximate solution and defining the geometrical mapping Φ . Approximation, stability and error estimates for h -refined IgA meshes of spatial computational domains can be found in [7], see also the monograph [10] for a comprehensive presentation of the IgA and its mathematical analysis. Using these approximation results for B-splines and NURBS, the V_{0h} -ellipticity of the discrete bilinear form $a_h(\cdot, \cdot)$ wrt the discrete norm $\|\cdot\|_h$, an appropriate boundedness result and the consistency, we derive asymptotically optimal discretization error estimate in the discrete norm $\|\cdot\|_h$. Furthermore, we consider moving spatial computational domains $\Omega(t) \subset \mathbb{R}^d$, $t \in [0, T]$, which always lead to a fix space-time cylinder $Q = \{(x, t) \in \mathbb{R}^{d+1} : x \in \Omega(t), t \in (0, T)\} \subset \mathbb{R}^{d+1}$ that can easily be discretized by IgA. We again derive a stable space-time IgA scheme and prove asymptotically optimal discretization error estimate in a similar discrete norm $\|\cdot\|_{h,m}$. Finally, we present a series of numerical experiments for fixed and moving spatial computational domains that support our theoretical results. Since the discrete bilinear form is V_{0h} -elliptic, one may expect that multigrid methods can efficiently solve the resulting space-time system of algebraic equation. Indeed, this is the case as one of our experiments with the standard AMG code hypre shows in Subsection 6.3, where we solve a linear system with 1.076.890.625 space-time unknowns (dofs) within 156 seconds using 16.384 cores. This results demonstrates the great potential of our discrete space-time formulation for the implementation on massively parallel computers.

The remainder of the paper is organized as follows: In Section 2, we recall the standard space-time variational formulations. Section 3 is devoted to the derivation of a stable space-time IgA discretization of our parabolic initial-boundary value problem. In Section 4, we derive our a priori discretization error estimate. Section 5 deals with the case of moving spatial computational domains. Our numerical results for fixed and moving spatial domains are presented and discussed in Section 6. Finally, we draw some conclusions in Section 7.

2 Space-Time Variational Formulations

Let us first introduce the Sobolev spaces $H^{l,k}(Q) = \{u \in L_2(Q) : \partial_x^\alpha u \in L_2(Q), \forall \alpha \text{ with } 0 \leq |\alpha| \leq l, \partial_t^i u \in L_2(Q), i = 0, \dots, k\}$ of functions defined in the space-time cylinder Q , where $L_2(Q)$ denotes the space of square-integrable functions, $\alpha = (\alpha_1, \dots, \alpha_d)$ is a multi-index with non-negative integers $\alpha_1, \dots, \alpha_d$, $|\alpha| = \alpha_1 + \dots + \alpha_d$, $\partial_x^\alpha u := \partial^{|\alpha|} u / \partial x^\alpha = \partial^{|\alpha|} u / \partial x_1^{\alpha_1} \dots \partial x_d^{\alpha_d}$ and $\partial_t^i u := \partial^i u / \partial t^i$, see, e.g., [29,30]. Furthermore, we need the spaces $H_0^{1,0}(Q) = \{u \in L_2(Q) : \nabla_x u \in [L_2(Q)]^d, u = 0 \text{ on } \Sigma\}$ and $H_{0,0}^{1,1}(Q) = \{u \in L_2(Q) : \nabla_x u \in [L_2(Q)]^d, \partial_t u \in L_2(Q), u = 0 \text{ on } \Sigma, \text{ and } u = 0 \text{ on } \Sigma_T\}$ for introducing the weak space-time formulation of (1.1), where $\Sigma_T := \Omega \times \{T\}$, and $\nabla_x u = (\partial u / \partial x_1, \dots, \partial u / \partial x_d)^\top$ denotes the gradient with respect to the spatial variables.

The standard weak space-time variational formulation of (1.1) reads as follows: find $u \in H_0^{1,0}(Q)$ such that

$$a(u, v) = l(v) \quad \forall v \in H_{0,0}^{1,1}(Q), \quad (2.1)$$

with the bilinear form

$$a(u, v) = - \int_Q u(x, t) \partial_t v(x, t) dx dt + \int_Q \nabla_x u(x, t) \cdot \nabla_x v(x, t) dx dt \quad (2.2)$$

and the linear form

$$l(v) = \int_Q f(x, t) v(x, t) dx dt + \int_\Omega u_0(x) v(x, 0) dx. \quad (2.3)$$

The variational problem (2.1) is known to have a unique weak solution [29,30]. In the later books, more general parabolic initial-boundary value problems, including other boundary conditions and more general elliptic parts, and non-linear versions are studied. Moreover, beside existence and uniqueness results, the reader also finds useful a priori estimates and regularity results, see also [53]. We here mention that time-stepping methods rather based on line variational formulations which are formulated in function spaces of abstract functions mapping the time interval $(0, T)$ into some Sobolev space of functions living on Ω , see, e.g., [57,59], [52], and [53] for the connection of these different formulations.

3 Stable Space-Time IgA Discretizations

In this section, we briefly recall the definitions of B-splines and NURBS basis functions and their use for both the geometrical representation of the

space-time cylinder Q and the construction of the IgA trial spaces where we look for approximate solutions to our variational parabolic evolution problem (2.1). For more details on B-splines and NURBS-based IgA, we refer to the monograph [10]. Then we derive our stable space-time IgA scheme that uniquely defines an approximate solution u_h in the IgA space. This approximate solution can be defined by solving one linear system of algebraic equations the solution of which is nothing but the vector \underline{u}_h of control points for u_h .

3.1 B-splines and NURBS

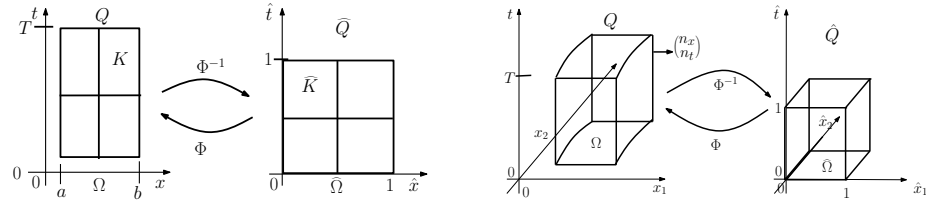


Fig. 1. Space-time IgA paraphernalia for $Q \subset \mathbb{R}^{d+1}$ with $d = 1$ (left) and $d = 2$ (right).

Let $p \geq 1$ denote the polynomial degree and n the number of basis functions defining the B-spline curve. Then a knot vector is nothing but a set of non-decreasing sequence of real numbers in the parameter domain and can be written as $\Xi = \{\xi_1, \dots, \xi_{n+p+1}\}$. By convention, we assume that $\xi_1 = 0$ and $\xi_{n+p+1} = 1$. We also note that the knot value may be repeated indicating its multiplicity m . We always consider open knot vectors, i.e., knot vectors where the first and last knot values appear $p + 1$ times, or, in other word, the multiplicity m of the first and last knots is $p + 1$. For the one-dimensional parametric domain $(0, 1)$, there is an underlying mesh $\hat{\mathcal{K}}_h$ consisting of elements \hat{K} created by the distinct knots. We denote the global mesh size by $\hat{h} := \max\{\hat{h}_K : \hat{K} \in \hat{\mathcal{K}}_h\}$, where $\hat{h}_K := \text{diam}(\hat{K}) = \text{length}(\hat{K})$. For the time being, we assume that the ratio of the sizes of neighboring elements is uniformly bounded from above and below. In this case, we speak about locally quasi-uniform meshes.

The univariate B-spline basis functions $\widehat{B}_{i,p} : (0,1) \rightarrow \mathbb{R}$ are recursively defined by means of the Cox-de Boor recursion formula as follows:

$$\widehat{B}_{i,0}(\xi) = \begin{cases} 1 & \text{if } \xi_i \leq \xi < \xi_{i+1}, \\ 0 & \text{else,} \end{cases} \quad (3.1)$$

$$\widehat{B}_{i,p}(\xi) = \frac{\xi - \xi_i}{\xi_{i+p} - \xi_i} \widehat{B}_{i,p-1}(\xi) + \frac{\xi_{i+p+1} - \xi}{\xi_{i+p+1} - \xi_{i+1}} \widehat{B}_{i+1,p-1}(\xi), \quad (3.2)$$

where a division by zero is defined to be zero. We note that a basis function of degree p is $(p - m)$ times continuously differentiable across a knot with the multiplicity m . If all internal knots have the multiplicity 1, then B-splines of degree p are globally C^{p-1} -continuous. In all numerical examples presented in Section 6, we exactly consider this case.

Now we define the multivariate B-spline basis functions on the space-time parameter domain $\widehat{Q} := (0,1)^{d+1} \subset \mathbb{R}^{d+1}$ with $d = 1, 2$, or 3 as product of the corresponding univariate B-spline basis functions. To do this, we first define the knot vectors $\Xi_\alpha = \{\xi_1^\alpha, \dots, \xi_{n_\alpha+p_\alpha+1}^\alpha\}$ for every space-time direction $\alpha = 1, \dots, d+1$. Furthermore, we introduce the multi-indices $i := (i_1, \dots, i_{d+1})$ and $p := (p_1, \dots, p_{d+1})$, the set $\overline{\mathcal{I}} = \{i = (i_1, \dots, i_{d+1}) : i_\alpha = 1, 2, \dots, n_\alpha; \alpha = 1, 2, \dots, d+1\}$. The product of the univariate B-spline basis functions now gives multivariate B-spline basis functions

$$\widehat{B}_{i,p}(\xi) := \prod_{\alpha=1}^{d+1} \widehat{B}_{i_\alpha, p_\alpha}(\xi_\alpha), \quad (3.3)$$

where $\xi = (\xi_1, \dots, \xi_{d+1}) \in \widehat{Q}$. The univariate and multivariate NURBS basis functions are defined in the parametric domain by means of the corresponding B-spline basis functions $\{\widehat{B}_{i,p}\}_{i \in \overline{\mathcal{I}}}$. For given $p = (p_1, \dots, p_{d+1})$ and for all $i \in \overline{\mathcal{I}}$, we define the NURBS basis function $\widehat{R}_{i,p}$ as follows:

$$\widehat{R}_{i,p} : (0,1) \rightarrow \mathbb{R}, \quad \widehat{R}_{i,p}(\xi) := \frac{\widehat{B}_{i,p}(\xi)w_i}{W(\xi)} \quad (3.4)$$

with the weighting function

$$W : (0,1) \rightarrow \mathbb{R}, \quad W(\xi) := \sum_{i \in \overline{\mathcal{I}}} w_i \widehat{B}_{i,p}(\xi), \quad (3.5)$$

where the weights w_i are positive real numbers.

The physical space-time computational domain $Q \subset \mathbb{R}^{d+1}$ is now defined from the parametric domain $\widehat{Q} = (0,1)^{d+1}$ by the geometrical mapping

$$\Phi : \widehat{Q} \rightarrow Q = \Phi(\widehat{Q}) \subset \mathbb{R}^{d+1}, \quad \Phi(\xi) = \sum_{i \in \overline{\mathcal{I}}} \widehat{R}_{i,p}(\xi) \mathbf{P}_i, \quad (3.6)$$

where $\widehat{R}_{i,p}$, $i \in \overline{\mathcal{I}}$, are the multivariate NURBS basis functions and $\{\mathbf{P}_i\}_{i \in \overline{\mathcal{I}}} \subset \mathbb{R}^{d+1}$ are the control points, see also Figure 1 as well as Figures 6 and 7 in Subsection 6.2.

By means of the geometrical mapping (3.6), we define the physical mesh \mathcal{K}_h , associated to the computational domain Q , whose vertices and elements are the images of the vertices and elements of the corresponding underlying mesh $\widehat{\mathcal{K}}_h$ in the parametric domain \widehat{Q} , i.e., $\mathcal{K}_h := \{K = \Phi(\widehat{K}) : \widehat{K} \in \widehat{\mathcal{K}}_h\}$. We denote the global mesh size of the mesh in the physical domain by $h := \max\{h_K : K \in \mathcal{K}_h\}$, with $h_K := \|\nabla\Phi\|_{L^\infty(K)} \widehat{h}_{\widehat{K}}$ and $\widehat{h}_{\widehat{K}} = \text{diam}(\widehat{K})$. Further, we assume that the physical mesh is quasi uniform, i.e., there exists a positive constant C_u , independent of h , such that

$$h_K \leq h \leq C_u h_K \quad \text{for all } K \in \mathcal{K}_h. \quad (3.7)$$

Finally, we define the NURBS space

$$V_h = \text{span}\{\varphi_{h,i} = \widehat{R}_{i,p} \circ \Phi^{-1}\}_{i \in \overline{\mathcal{I}}} \quad (3.8)$$

on Q by a push-forward of the NURBS basis functions, where we assumed that the geometrical mapping Φ is invertible a.e. in Q , with smooth inverse on each element K of the physical mesh $K \in \mathcal{K}_h$, see [7] and [47] for more details.

Furthermore, we introduce the subspace

$$V_{0h} := V_h \cap H_{0,\underline{0}}^{1,1}(Q) = \{v_h \in V_h : v_h|_{\Sigma \cup \Sigma_0} = 0\} = \text{span}\{\varphi_{h,i}\}_{i \in \mathcal{I}} \quad (3.9)$$

of all functions from V_h fulfilling homogeneous boundary and initial conditions. For simplicity, we below assume the same polynomial degree for all coordinate directions, i.e. $p_\alpha = p$ for all $\alpha = 1, 2, \dots, d+1$.

3.2 Discrete Space-Time Variational Problem

In order to derive our discrete scheme for defining an approximate solution $u_h \in V_{0h}$, we multiply our parabolic PDE (1.1) by a time-upwind test function of the form $v_h + \theta h \partial_t v_h$ with an arbitrary $v_h \in V_{0h} \subset H_{0,\underline{0}}^{1,1}(Q)$ and a positive constant θ which will be defined later, and integrate over the whole space-time cylinder Q , giving the identity

$$\begin{aligned} & \int_Q (\partial_t u_h v_h + \theta h \partial_t u_h \partial_t v_h - \Delta u_h (v_h + \theta h \partial_t v_h)) \, dxdt \\ &= \int_Q f(v_h + \theta h \partial_t v_h) \, dxdt \end{aligned} \quad (3.10)$$

that is formally valid for all $v_h \in V_{0h} \subset H_{0,0}^{2,1}(Q)$. Integration by parts with respect to x in the last term of the bilinear form on the left-hand side of (3.10) gives

$$\begin{aligned} & \int_Q (\partial_t u_h v_h + \theta h \partial_t u_h \partial_t v_h + \nabla_x u_h \cdot \nabla_x v_h + \theta h \nabla_x u_h \cdot \nabla_x \partial_t v_h) dx dt \\ & - \int_{\partial Q} n_x \cdot \nabla_x u_h (v_h + \theta h \partial_t v_h) ds = \int_Q f v_h dx dt + \theta h \int_Q f \partial_t v_h dx dt. \end{aligned}$$

We mention that $\partial_t v_h$ is differentiable wrt x due to the special tensor product structure of V_{0h} . Using the facts that v_h and $\partial_t v_h$ are always zero on Σ , and the x -components $n_x = (n_1, \dots, n_d)^\top$ of the normal $n = (n_1, \dots, n_d, n_{d+1})^\top = (n_x, n_t)^\top$ is zero on Σ_0 and Σ_T , we arrive at our discrete scheme: find $u_h \in V_{0h}$ such that

$$a_h(u_h, v_h) = l_h(v_h) \quad \forall v_h \in V_{0h}, \quad (3.11)$$

where

$$\begin{aligned} a_h(u_h, v_h) = & \int_Q (\partial_t u_h v_h + \theta h \partial_t u_h \partial_t v_h \\ & + \nabla_x u_h \nabla_x v_h + \theta h \nabla_x u_h \cdot \nabla_x \partial_t v_h) dx dt, \end{aligned} \quad (3.12)$$

$$l_h(v_h) = \int_Q f [v_h + \theta h \partial_t v_h] dx dt, \quad (3.13)$$

and θ is a positive constant which will be determined later.

Next we will show that the discrete bilinear form (3.12) is V_{0h} -coercive with respect to the discrete norm

$$\|v_h\|_h = \left[\|\nabla_x v_h\|_{L_2(Q)}^2 + \theta h \|\partial_t v_h\|_{L_2(Q)}^2 + \frac{1}{2} \|v_h\|_{L_2(\Sigma_T)}^2 \right]^{1/2}. \quad (3.14)$$

Remark 1. We note that (3.14) is a norm on V_{0h} . Indeed, if $\|v_h\|_h = 0$ for some $v_h \in V_{0h}$, then we have $\nabla_x v_h = 0$ and $\partial_t v_h = 0$ in Q and also $v_h = 0$ on Σ_T . This means that the function v_h is constant in the space-time cylinder Q . Since $v_h = 0$ on the boundary Σ_T and all functions of the discrete space V_{0h} are continuous, we conclude that $v_h = 0$ in the whole space-time domain Q . The other norm axioms are obviously fulfilled.

Lemma 1. *The discrete bilinear form $a_h(\cdot, \cdot) : V_{0h} \times V_{0h} \rightarrow \mathbb{R}$, defined by (3.12), is V_{0h} -coercive wrt the norm $\|\cdot\|_h$, i.e.*

$$a_h(v_h, v_h) \geq \mu_c \|v_h\|_h^2, \quad \forall v_h \in V_{0h} \quad (3.15)$$

with $\mu_c = 1$.

Proof. Using Gauss' theorem and the fact that $n_t = 0$ on Σ , we get

$$\begin{aligned} a_h(v_h, v_h) &= \int_Q (\partial_t v_h v_h + \theta h (\partial_t v_h)^2 + \nabla_x v_h \cdot \nabla_x v_h + \theta h \nabla_x v_h \cdot \nabla_x \partial_t v_h) dx dt \\ &= \int_Q \left[\frac{1}{2} \partial_t v_h^2 + \theta h (\partial_t v_h)^2 + |\nabla_x v_h|^2 + \frac{\theta h}{2} \partial_t |\nabla_x v_h|^2 \right] dx dt \\ &= \frac{1}{2} \int_{\partial Q} v_h^2 n_t ds + \theta h \|\partial_t v_h\|_{L_2(Q)}^2 + \|\nabla_x v_h\|_{L_2(Q)}^2 + \frac{\theta h}{2} \int_{\partial Q} |\nabla_x v_h|^2 n_t ds \\ &= \frac{1}{2} \left(\|v_h\|_{L_2(\Sigma_T)}^2 - \|v_h\|_{L_2(\Sigma_0)}^2 \right) + \theta h \|\partial_t v_h\|_{L_2(Q)}^2 + \|\nabla_x v_h\|_{L_2(Q)}^2 \\ &\quad + \frac{\theta h}{2} \left(\|\nabla_x v_h\|_{L_2(\Sigma_T)}^2 - \|\nabla_x v_h\|_{L_2(\Sigma_0)}^2 \right) \end{aligned}$$

for all $v_h \in V_{0h}$. Since $v_h(x, 0) = 0$ and, therefore, $\nabla_x v_h(x, 0) = 0$ for all $x \in \overline{\Omega}$, i.e., $v_h = 0$ and $\nabla_x v_h = 0$ on Σ_0 , we immediately arrive at the estimate

$$\begin{aligned} a_h(v_h, v_h) &= \frac{1}{2} \|v_h\|_{L_2(\Sigma_T)}^2 + \theta h \|\partial_t v_h\|_{L_2(Q)}^2 + \|\nabla_x v_h\|_{L_2(Q)}^2 + \frac{\theta h}{2} \|\nabla_x v_h\|_{L_2(\Sigma_T)}^2 \\ &\geq \frac{1}{2} \|v_h\|_{L_2(\Sigma_T)}^2 + \theta h \|\partial_t v_h\|_{L_2(Q)}^2 + \|\nabla_x v_h\|_{L_2(Q)}^2 \\ &= \|v_h\|_h^2 \quad \forall v \in V_{0h}, \end{aligned}$$

which proves our lemma. \square

Lemma 1 immediately yields that the solution $u_h \in V_{0h}$ of (3.11) is unique. Indeed, let us assume that there is another solution $\tilde{u}_h \in V_{0h}$ such that $a_h(\tilde{u}_h, v_h) = l_h(v_h)$ for all $v_h \in V_{0h}$. Then, taking the difference, we get $a_h(u_h - \tilde{u}_h, v_h) = 0$ for all $v_h \in V_{0h}$. Choosing $v_h = u_h - \tilde{u}_h \in V_{0h}$ and applying Lemma 1, we immediately obtain the estimate $0 \leq \|u_h - \tilde{u}_h\|_h^2 \leq a_h(u_h - \tilde{u}_h, u_h - \tilde{u}_h) = 0$, i.e., $u_h - \tilde{u}_h = 0$. Thus, the solution is unique. Since the discrete variational problem (3.11) is posed in the finite dimensional space V_{0h} , the uniqueness yields existence of the solution $u_h \in V_{0h}$ of (3.11).

Since we already choose the standard B-spline resp. NURBS basis of V_{0h} in (3.9) as $V_{0h} = \text{span}\{\varphi_{h,i}\}_{i \in \mathcal{I}}$, we look for the solution $u_h \in V_{0h}$ of (3.11) in the form of

$$u_h(x, t) = u_h(x_1, \dots, x_d, x_{d+1}) = \sum_{i \in \mathcal{I}} u_i \varphi_{h,i}(x, t)$$

where $\underline{u}_h := [u_i]_{i \in \mathcal{I}} \in \mathbb{R}^{N_h = |\mathcal{I}|}$ is the unknown vector of control points defined by the solution of the system of algebraic equations

$$K_h \underline{u}_h = \underline{f}_h, \quad (3.16)$$

with the $N_h \times N_h$ system matrix $K_h = [K_{\mathbf{ij}} = a_h(\varphi_{h,j}, \varphi_{h,i})]_{i,j \in \mathcal{I}}$ and the right-hand side $\underline{f}_h = [f_{\mathbf{i}} = l_h(\varphi_{h,i})]_{i \in \mathcal{I}} \in \mathbb{R}^{N_h}$ that can be generated as in a usual IgA code for elliptic problems. It is again clear from Lemma 1 that the stiffness matrix is regular.

In the next section, we derive an a-priori discretization error estimate wrt the $\|\cdot\|_h$ norm.

4 Discretization Error Analysis

At first, we will present the main ingredients, which are necessary for the derivation of our a priori discretization error estimate, in form of Lemmas.

Lemma 2. *Let $K = \Phi(\widehat{K}) \in \mathcal{K}_h$ and $\widehat{K} \in \widehat{\mathcal{K}}_h$. Then the scaled trace inequality*

$$\|v\|_{L_2(\partial K)} \leq C_{tr} h_K^{-1/2} (\|v\|_{L_2(K)} + h_K |v|_{H^1(K)}) \quad (4.1)$$

holds for all $v \in H^1(K)$, where h_K denotes the mesh size of K in the physical domain, and C_{tr} is a positive constant that only depends on the shape regularity of the mapping Φ and the constant C in the trace inequality

$$\|f\|_{L_2(\partial(0,1)^{d+1})} \leq C \|f\|_{H^1((0,1)^{d+1})} \quad (4.2)$$

that is valid for all $f \in H^1((0,1)^{d+1})$.

Proof. The proof follows from (4.2) by mapping and scaling similar to the proof of [12, Theorem 3.2], where (4.1) is proved for $d = 2$ in such a way that the structure of the constants C_{tr} is explicitly given. \square

Lemma 3. *Let K be an arbitrary mesh element from \mathcal{K}_h . Then the inverse inequalities*

$$\|\nabla v_h\|_{L_2(K)} \leq C_{inv,1} h_K^{-1} \|v_h\|_{L_2(K)} \quad (4.3)$$

and

$$\|v_h\|_{L_2(\partial K)} \leq C_{inv,0} h_K^{-1/2} \|v_h\|_{L_2(K)} \quad (4.4)$$

hold for all $v_h \in V_h$, where $C_{inv,1}$ and $C_{inv,0}$ are positive constants, which are independent of h_K and $K \in \mathcal{K}_h$.

Proof. The inverse inequality (4.3) is a special case of the inverse inequalities given in [7, Theorem 4.1] and [7, Theorem 4.2]. The proof of (4.4) can be found in [12, Theorem 4.1]. \square

We note that estimate (4.3) immediately implies the inverse inequality

$$\|\partial_t v_h\|_{L_2(K)} \leq C_{inv,1} h_K^{-1} \|v_h\|_{L_2(K)} \quad \forall v_h \in V_h,$$

because ∂_t is a part of $\nabla = (\nabla_x, \partial_t)^\top$. Below we need the inverse inequality

$$\|\partial_t \partial_{x_i} v_h\|_{L_2(K)} \leq C_{inv,1} h_K^{-1} \|\partial_{x_i} v_h\|_{L_2(K)} \quad (4.5)$$

that is obviously valid for all $v_h \in V_h$ and $i = 1, \dots, d$ as well.

To prove the a priori error estimate, we need to show the uniform boundedness of the discrete bilinear form $a_h(\cdot, \cdot)$ on $V_{0h,*} \times V_{0h}$, where the space $V_{0h,*} = H_0^{1,0}(Q) \cap H^{2,1}(Q) + V_{0h}$ is equipped with the norm

$$\|v\|_{h,*} = \left[\|v\|_h^2 + (\theta h)^{-1} \|v_h\|_{L_2(Q)}^2 \right]^{1/2}. \quad (4.6)$$

Lemma 4. *The discrete bilinear form $a_h(\cdot, \cdot)$, defined by (3.12), is uniformly bounded on $V_{0h,*} \times V_{0h}$, i.e., there exists a positive constant μ_b that does not depend on h such that*

$$|a_h(u, v_h)| \leq \mu_b \|u\|_{h,*} \|v_h\|_h, \quad \forall u \in V_{0h,*}, \forall v_h \in V_{0h}. \quad (4.7)$$

Proof. Let us estimate the bilinear form (3.12)

$$a_h(u, v_h) = \int_Q (\partial_t u v_h + \theta h \partial_t u \partial_t v_h + \nabla_x u \cdot \nabla_x v_h + \theta h \nabla_x u \cdot \nabla_x \partial_t v_h) dx dt,$$

term by term.

For the first term, since $V_{0h} \subset H_{0,\mathbf{Q}}^{1,1}$, we can proceed with an integration by parts wrt t , and then estimate the resulting terms by Cauchy-Schwarz inequality as follows:

$$\begin{aligned} \int_Q \partial_t u_h v_h \, dxdt &= - \int_Q u \partial_t v_h \, dxdt + \int_{\Sigma_T} u v_h \, ds \\ &\leq \left[(\theta h)^{-1} \|u\|_{L_2(Q)}^2 \right]^{\frac{1}{2}} \left[\theta h \|\partial_t v_h\|_{L_2(Q)}^2 \right]^{\frac{1}{2}} \\ &\quad + \left[\|u\|_{L_2(\Sigma_T)}^2 \right]^{\frac{1}{2}} \left[\|v_h\|_{L_2(\Sigma_T)}^2 \right]^{\frac{1}{2}}. \end{aligned}$$

The second and third term of (3.12) can easily be bounded by means of Cauchy's inequality as follows:

$$\theta h \int_Q \partial_t u \partial_t v_h \, dxdt \leq \left[\theta h \|\partial_t u\|_{L_2(Q)}^2 \right]^{\frac{1}{2}} \left[\theta h \|\partial_t v_h\|_{L_2(Q)}^2 \right]^{\frac{1}{2}}.$$

and

$$\int_Q \nabla_x u \cdot \nabla_x v_h \, dxdt \leq \left[\|\nabla_x u\|_{L_2(Q)}^2 \right]^{\frac{1}{2}} \left[\|\nabla_x v_h\|_{L_2(Q)}^2 \right]^{\frac{1}{2}}.$$

The final term in the bilinear form is bounded from above by applying the Cauchy-Schwarz inequality, inverse inequality (4.5), and inequality (3.7) to obtain

$$\begin{aligned} \theta h \int_Q \nabla_x u_h \cdot \nabla_x \partial_t v_h \, dxdt &\leq \left[\|\nabla_x u\|_{L_2(Q)}^2 \right]^{\frac{1}{2}} \left[(\theta h)^2 \|\partial_t \nabla_x v_h\|_{L_2(Q)}^2 \right]^{\frac{1}{2}} \\ &= \left[\|\nabla_x u\|_{L_2(Q)}^2 \right]^{\frac{1}{2}} \left[(\theta h)^2 \sum_{i=1}^d \sum_{K \in \mathcal{K}_h} \|\partial_t (\partial_{x_i} v_h)\|_{L_2(K)}^2 \right]^{\frac{1}{2}} \\ &\leq \left[\|\nabla_x u\|_{L_2(Q)}^2 \right]^{\frac{1}{2}} \left[(\theta h)^2 C_{inv,1}^2 \sum_{i=1}^d \sum_{K \in \mathcal{K}_h} h_K^{-2} \|\partial_{x_i} v_h\|_{L_2(K)}^2 \right]^{\frac{1}{2}} \\ &\leq \left[\|\nabla_x u\|_{L_2(Q)}^2 \right]^{\frac{1}{2}} \left[C_u^2 C_{inv,1}^2 \theta^2 \|\nabla_x v_h\|_{L_2(Q)}^2 \right]^{\frac{1}{2}}. \end{aligned}$$

Combining the terms from above and using Cauchy's inequality, we get

$$\begin{aligned}
a_h(u_h, v_h) &\leq \left[(\theta h)^{-1} \|u\|_{L_2(Q)}^2 + \|u\|_{L_2(\Sigma_T)}^2 \right. \\
&\quad \left. + \theta h \|\partial_t u\|_{L_2(Q)}^2 + \|\nabla_x u\|_{L_2(Q)}^2 + \|\nabla_x u\|_{L_2(Q)}^2 \right]^{\frac{1}{2}} \\
&\quad \times \left[\theta h \|\partial_t v_h\|_{L_2(Q)}^2 + \|v_h\|_{L_2(\Sigma_T)}^2 + \theta h \|\partial_t v_h\|_{L_2(Q)}^2 \right. \\
&\quad \left. + \|\nabla_x v_h\|_{L_2(Q)}^2 + C_u^2 C_{inv,1}^2 \theta^2 \|\nabla_x v_h\|_{L_2(Q)}^2 \right]^{\frac{1}{2}} \\
&\leq \left[2\|\nabla_x u\|_{L_2(Q)}^2 + \theta h \|\partial_t u\|_{L_2(Q)}^2 + (\theta h)^{-1} \|u\|_{L_2(Q)}^2 + \|u\|_{L_2(\Sigma_T)}^2 \right]^{\frac{1}{2}} \\
&\quad \times \left[(1 + C_u^2 C_{inv,1}^2 \theta^2) \|\nabla_x v_h\|_{L_2(Q)}^2 + 2\theta h \|\partial_t v_h\|_{L_2(Q)}^2 + \|v_h\|_{L_2(\Sigma_T)}^2 \right]^{\frac{1}{2}} \\
&\leq \mu_b \|u\|_{h,*} \|v_h\|_h,
\end{aligned}$$

where $\mu_b = (2 \max\{(1 + C_u^2 C_{inv,1}^2 \theta^2)/2, 1\})^{1/2}$. \square

Next we recall some approximation properties of our B-spline resp. NURBS space that follow from the approximation results proved in [7, Section 3] and [47, Section 3]. Indeed, there exists projective operators $\Pi_h : L_2(Q) \rightarrow V_h$ that deliver the corresponding asymptotically optimal approximation results.

Lemma 5. *Let l and s be integers with $0 \leq l \leq s \leq p + 1$, and let $v \in H^s(Q) \cap H_{0,\underline{0}}^{1,1}(Q)$. Then there exist a projective operator Π_h from $H_{0,\underline{0}}^{1,1}(Q) \cap H^s(Q)$ to V_{0h} and a positive generic constant C_s such that*

$$\sum_{K \in \mathcal{K}_h} |v - \Pi_h v|_{H^1(K)}^2 \leq C_s h^{2(s-l)} \|v\|_{H^s(Q)}^2, \quad (4.8)$$

where h again denotes the mesh-size parameter in the physical domain, p denotes the underlying polynomial degree of the B-spline resp. NURBS, and the generic constant C_s only depends on l, s and p , the shape regularity of the physical space-time domain Q described by the mapping Φ and, in particular, the gradient $\nabla \Phi$ of the mapping Φ , but not on h and v .

Proof. The proof follows the proof of the approximation results presented in Subsections 3.3 and 3.4 of [7], see also [47, Proposition 3.1]. \square

If $\Pi_h v$ belongs to $V_{0h} \cap H^l(Q)$ (the multiplicity of the inner knots is not larger than $p + 1 - l$), then estimate (4.8) immediately yields the global estimate

$$|v - \Pi_h v|_{H^l(Q)} \leq C_s^{0.5} h^{(s-l)} \|v\|_{H^s(Q)}. \quad (4.9)$$

The basic approximation estimates (4.8) and (4.9) yield estimates of the approximation error $v - \Pi_h v$ wrt to the $\|\cdot\|_{L_2(\partial Q)}$ - norm as well as wrt to the discrete norms $\|\cdot\|_h$ and $\|\cdot\|_{h,*}$ which we later need in estimation of the discretization error $u - u_h$.

Lemma 6. *Let s be a positive integer with $1 \leq s \leq p + 1$, and let $v \in H^s(Q) \cap H_{0,\underline{0}}^{1,1}(Q)$. Then there exist a projection Π_h from $H_{0,\underline{0}}^{1,1}(Q)$ to V_{0h} and generic positive constants C_1 , C_2 and C_3 such that*

$$\|v - \Pi_h v\|_{L_2(\partial Q)} \leq C_1 h^{s-1/2} \|v\|_{H^s(Q)}, \quad (4.10)$$

$$\|v - \Pi_h v\|_h \leq C_2 h^{s-1} \|v\|_{H^s(Q)}, \quad (4.11)$$

$$\|v - \Pi_h v\|_{h,*} \leq C_3 h^{s-1} \|v\|_{H^s(Q)}, \quad (4.12)$$

where h is the mesh-size parameter in the physical domain, p denotes the underlying polynomial degree of the B-spline resp. NURBS, and the generic constants C_1 , C_2 and C_3 only depends on l, s and p , the shape regularity of the physical space-time domain Q described by the mapping Φ and, in particular, the gradient $\nabla\Phi$ of the mapping Φ , but not on h and v .

Proof. By applying inequality (4.1), the quasi uniformity assumption (3.7) and Lemma 5, the proof of (4.10) is obtained as follows:

$$\begin{aligned} \|v - \Pi_h v\|_{L_2(\partial Q)}^2 &= \sum_{\substack{K \in \mathcal{K}_h \\ \partial K \cap \partial Q \neq \emptyset}} \|v - \Pi_h v\|_{L_2(\partial K \cap \partial Q)}^2 \\ &\leq 2C_{tr}^2 \sum_{K \in \mathcal{K}_h} \left(h_K^{-1} \|v - \Pi_h v\|_{L_2(K)}^2 + h_K |v - \Pi_h v|_{H^1(K)}^2 \right) \\ &\leq 2C_{tr}^2 \sum_{K \in \mathcal{K}_h} \left(C_u h^{-1} \|v - \Pi_h v\|_{L_2(K)}^2 + h |v - \Pi_h v|_{H^1(K)}^2 \right) \\ &\leq 2C_{tr}^2 \left(C_u h^{-1} \|v - \Pi_h v\|_{L_2(Q)}^2 + h |v - \Pi_h v|_{H^1(Q)}^2 \right) \\ &\leq 2C_{tr}^2 \left(C_u h^{-1} C_s h^{2s} + h C_s h^{2(s-1)} \right) \|v\|_{H^s(Q)}^2 \\ &\leq 2C_{tr}^2 C_s (C_u + 1) h^{2s-1} \|v\|_{H^s(Q)}^2 = C_1 h^{2s-1} \|v\|_{H^s(Q)}^2. \end{aligned}$$

The definition (3.14) of the norm $\|\cdot\|_h$, the approximation error estimate (4.8) for $l = 1$, and the estimate (4.10) just proved yield

$$\begin{aligned} \|v - \Pi_h v\|_h^2 &= \|\nabla_x(v - \Pi_h v)\|_{L_2(Q)}^2 + \theta h \|\partial_t(v - \Pi_h v)\|_{L_2(Q)}^2 \\ &\quad + \frac{1}{2} \|v - \Pi_h v\|_{L_2(\Sigma_T)}^2 \\ &\leq \left(C_s h^{2(s-1)} + \theta h C_s h^{2(s-1)} + 1/2 h C_1^2 h^{2(s-1)} \right) \|v\|_{H^s(Q)}^2 \\ &= (C_s + C_s \theta h + \frac{C_1}{2} h^2) h^{2(s-1)} \|v\|_{H^s(Q)}^2 = C_2 h^{2(s-1)} \|v\|_{H^s(Q)}^2, \end{aligned}$$

which proves the second estimate of Lemma 6. Now let us prove the last estimate. Using the definition of the norm (4.6), the just proven estimate (4.11), and the approximation error estimate (4.8) for $l = 0$, we get

$$\begin{aligned} \|v - \Pi_h v\|_{h,*}^2 &= \|v - \Pi_h v\|_h^2 + (\theta h)^{-1} \|v - \Pi_h v\|_{L_2(Q)}^2 \\ &\leq \left(C_2 h^{2(s-1)} + (\theta h)^{-1} C_s h^{2s} \right) \|v\|_{H^s(Q)}^2 \\ &= (C_2 + \theta^{-1} h C_s) h^{2(s-1)} \|v\|_{H^s(Q)}^2 = C_3 h^{2(s-1)} \|v\|_{H^s(Q)}^2, \end{aligned}$$

which completes the proof of the lemma. \square

Lemma 7. *If the solution $u \in H_0^{1,0}(Q)$ of the variational problem (2.1) belongs to $H^{2,1}(Q)$, then it satisfies the consistency identity*

$$a_h(u, v_h) = l_h(v_h) \quad \forall v_h \in V_{0h}. \quad (4.13)$$

Proof. Since $u \in H_0^{1,0}(Q) \cap H^{2,1}(Q)$, integration by parts in (2.1) wrt t and x gives the variational identity

$$\begin{aligned} \int_Q f v \, dx dt + \int_{\Sigma_0} u_0 v \, ds &= \int_Q (\partial_t u - \Delta u) v \, dx dt - \int_{\partial Q} n_t u v \, ds + \int_{\partial Q} n_x \cdot \nabla_x u v \, ds \\ &= \int_Q (\partial_t u - \Delta u) v \, dx dt - \int_{\Sigma_T} u v \, ds + \int_{\Sigma_0} u v \, ds + \int_{\partial Q} n_x \cdot \nabla_x u v \, ds \\ &= \int_Q (\partial_t u - \Delta u) v \, dx dt + \int_{\Sigma_0} u v \, ds \quad \forall v \in H_{0,0}^{1,1}(Q). \end{aligned} \quad (4.14)$$

If we take a test function $v \in C_0^\infty(Q) \subset H_{0,0}^{1,1}(Q)$, then it follows that

$$\int_Q f v \, dx dt = \int_Q (\partial_t u - \Delta u) v \, dx dt.$$

Since $C_0^\infty(Q)$ is dense in $L_2(Q)$, we have

$$\partial_t u - \Delta u = f \quad \text{in } L_2(Q).$$

From (4.14), we now conclude that

$$\int_{\Sigma_0} u_0 v \, ds = \int_{\Sigma_0} uv \, ds$$

for all $v \in H_{0,0}^{1,1}(Q)$, i.e., $u = u_0$ on Σ_0 . Since $u \in H_0^{1,0}(Q)$, the Dirichlet trace of u on Σ is zero. This gives us the strong form of our model problem (1.1).

Now, multiplying $\partial_t u - \Delta u = f$ by a test function $v_h + \theta h \partial_t v_h$, where $v_h \in V_{0h}$, integrating over Q , we get

$$\int_Q (\partial_t u - \Delta u)(v_h + \theta h \partial_t v_h) \, dxdt = \int_Q f(v_h + \theta h \partial_t v_h) \, dxdt \quad \forall v_h \in V_{0h}.$$

Integrating by parts wrt x gives

$$\begin{aligned} & \int_Q \partial_t u(v_h + \theta h \partial_t v_h) \, dxdt + \nabla_x u \cdot \nabla_x(v_h + \theta h \partial_t v_h) \, dxdt \\ & - \int_{\partial Q} n_x \cdot \nabla_x u(v_h + \theta h \partial_t v_h) \, ds = \int_Q f(v_h + \theta h \partial_t v_h) \, dxdt. \end{aligned}$$

Using the fact that $n_x = 0$ on both Σ_0 and Σ_T , and $v_h \in V_{0h}$, we have

$$\begin{aligned} & \int_Q \partial_t u(v_h + \theta h \partial_t v_h) \, dxdt + \nabla_x u \cdot \nabla_x(v_h + \theta h \partial_t v_h) \, dxdt \\ & = \int_Q f(v_h + \theta h \partial_t v_h) \, dxdt, \end{aligned}$$

which completes the proof. \square

Now we are in the position to prove the main result for this section, namely the a priori discretization error estimate in the discrete norm $\|\cdot\|_h$.

Theorem 1. *Let $u \in H_0^{1,0}(Q) \cap H^s(Q)$ with $s \geq 2$ be the exact solution of our model problem (2.1), and let $u_h \in V_{0h}$ be the solution to the IgA scheme (3.11). Then the discretization error estimate*

$$\|u - u_h\|_h \leq Ch^{t-1} \|u\|_{H^t(Q)}, \quad (4.15)$$

holds, where C is a generic positive constant, $t = \min\{s, p + 1\}$, and p denotes the underlying polynomial degree of the B-splines or NURBS.

Proof. Subtracting the IgA scheme

$$a_h(u_h, v_h) = l_h(v_h), \quad \forall v_h \in V_{0h}$$

from the consistence identity

$$a_h(u, v_h) = l_h(v_h), \quad \forall v_h \in V_{0h},$$

we obtain the so-called Galerkin orthogonality

$$a_h(u - u_h, v_h) = 0, \quad \forall v_h \in V_{0h}, \quad (4.16)$$

that is crucial for the discretization error estimate.

Using now the triangle inequality, we can estimate the discretization error $u - u_h$ as follows

$$\|u - u_h\|_h \leq \|u - \Pi_h u\|_h + \|\Pi_h u - u_h\|_h. \quad (4.17)$$

The first term is nothing but the quasi-interpolation error that can easily be estimated by means of Lemma 6. The estimation of the second term on the right-hand side of (4.17) is more involved. Using the fact that $\Pi_h u - u_h \in V_{0h}$, the V_{0h} -ellipticity of the bilinear form $a_h(\cdot, \cdot)$ as was shown in Lemma 1, the Galerkin orthogonality (4.16), and the boundedness of the discrete bilinear form Lemma 4, we can derive the following estimates

$$\begin{aligned} \mu_c \|\Pi_h u - u_h\|_h^2 &\leq a_h(\Pi_h u - u_h, \Pi_h u - u_h) \\ &= a_h(\Pi_h u - u, \Pi_h u - u_h) \\ &\leq \mu_b \|\Pi_h u - u\|_{h,*} \|\Pi_h u - u_h\|_h. \end{aligned}$$

Hence, we have

$$\|\Pi_h u - u_h\|_h \leq (\mu_b / \mu_c) \|\Pi_h u - u\|_{h,*}. \quad (4.18)$$

Inserting (4.18) into the triangle inequality (4.17) and using the estimates (4.12) and (4.11) from Lemma 6, we have

$$\begin{aligned} \|u - u_h\|_h &\leq \|u - \Pi_h u\|_h + \|\Pi_h u - u_h\|_h \\ &\leq \|u - \Pi_h u\|_h + (\mu_b/\mu_c) \|\Pi_h u - u\|_{h,*} \\ &\leq C_s(1 + \mu_b/\mu_c) h^{t-1} \|v\|_{H^s(Q)}, \end{aligned}$$

which proves the discretization error estimate 4.15 with $C = C_s(1 + \mu_b/\mu_c)$. \square

5 Moving Spatial Computational Domain

In this section, we will formulate the space-time scheme for a moving spatial domain $Q := \{(x, t) \in \mathbb{R}^{d+1}; x \in \Omega(t), t \in (0, T)\}$, where $\Omega(t) \subset \mathbb{R}^d$ for $d = 1, 2, 3$.

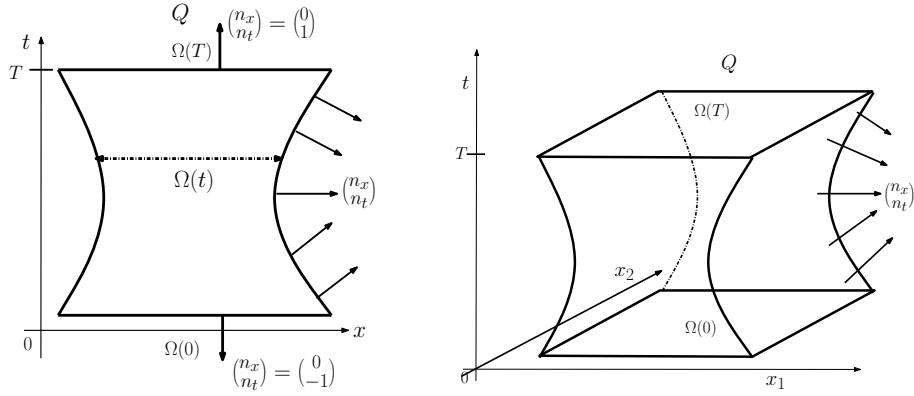


Fig. 2. Moving spatial domain $\Omega(t)$, $t \in [0, T]$.

Let us now assume that the underlying polynomial degree $p \geq 2$ and the multiplicity m of all internal knots is less than or equal $p - 1$, i.e., V_{0h} is always a subset of $C^1(\overline{Q})$. Thus, the IgA (B-spline or NURBS) space V_{0h} is a subspace of $H_{0,0}^{1,1}(Q) \cap H^2(Q)$. Similar to Subsection 3.2, we derive the IgA scheme by multiplying our parabolic PDE (1.1) by a test function of the form $v_h + \theta h \partial_t v_h$ with an arbitrary $v_h \in V_{0h}$, where θ is a positive constant which will be defined later, and integrating over

the whole space-time cylinder Q , giving the identity

$$\begin{aligned} \int_Q f(v_h + \theta h \partial_t v_h) \, dxdt &= \int_Q (\partial_t u_h v_h + \theta h \partial_t u_h \partial_t v_h) \, dxdt \\ &\quad - \Delta u_h (v_h + \theta h \partial_t v_h) \, dxdt \end{aligned} \quad (5.1)$$

that is valid for all $v_h \in V_{0h}$.

Integration by parts with respect to x in the last term of the bilinear form on the right-hand side of (5.1) gives

$$\begin{aligned} \int_Q f(v_h + \theta h \partial_t v_h) \, dxdt &= \int_Q (\partial_t u_h v_h + \theta h \partial_t u_h \partial_t v_h + \nabla_x u_h \cdot \nabla_x v_h \\ &\quad + \theta h \nabla_x u_h \cdot \nabla_x \partial_t v_h) \, dxdt - \int_{\partial Q} n_x \cdot \nabla_x u (v_h + \theta h \partial_t v_h) \, ds. \end{aligned}$$

We now integrate the fourth term on the right-hand side by parts wrt time t and obtain

$$\begin{aligned} &= \int_Q (\partial_t u_h v_h + \theta h \partial_t u_h \partial_t v_h + \nabla_x u_h \cdot \nabla_x v_h - \theta h \partial_t \nabla_x u_h \cdot \nabla_x v_h) \, dxdt \\ &\quad + \int_{\partial Q} n_t \nabla_x u_h \cdot \nabla_x v_h \, ds - \int_{\partial Q} n_x \cdot \nabla_x u_h (v_h + \theta h \partial_t v_h) \, ds. \end{aligned}$$

Using the facts that $v_h \in V_{0h}$ and n_x is zero on $\Sigma_0 \cup \Sigma_T$, we can continue to write

$$\begin{aligned} &= \int_Q (\partial_t u_h v_h + \theta h \partial_t u_h \partial_t v_h + \nabla_x u_h \cdot \nabla_x v_h - \theta h \partial_t \nabla_x u_h \cdot \nabla_x v_h) \, dxdt \\ &\quad + \theta h \int_{\Sigma \cup \Sigma_T} n_t \nabla_x u_h \cdot \nabla_x v_h \, ds - \theta h \int_{\Sigma} n_x \cdot \nabla_x u_h \partial_t v_h \, ds. \end{aligned}$$

Considering the terms on the boundary Σ , we note the following

$$\begin{aligned} &\theta h \int_{\Sigma} [n_t \nabla_x u_h \cdot \nabla_x v_h - n_x \cdot \nabla_x u_h \partial_t v_h] \, ds \\ &= \theta h \int_{\Sigma} \nabla_x u_h \cdot [n_t \nabla_x v_h - n_x \partial_t v_h] \, ds = 0, \end{aligned}$$

since $[n_t \nabla_x v_h - n_x \partial_t v_h]$ is the tangential derivative of v_h and $v_h = 0$ on Σ . Finally, we arrive at our discrete scheme: find $u_h \in V_{0h}$ such that

$$b_h(u_h, v_h) = l_h(v_h) \quad \forall v_h \in V_{0h}, \quad (5.2)$$

where the bilinear and linear forms are given as follows:

$$\begin{aligned} b_h(u_h, v_h) &:= \int_Q (\partial_t u_h v_h + \theta h \partial_t u_h \partial_t v_h + \nabla_x u_h \cdot \nabla_x v_h \\ &\quad - \theta h \partial_t \nabla_x u_h \cdot \nabla_x v_h) dxdt + \theta h \int_{\Sigma_T} \nabla_x u_h \cdot \nabla_x v_h ds, \quad (5.3) \\ l_h(v_h) &:= \int_Q f [v_h + \theta h \partial_t v_h] dxdt. \end{aligned}$$

Remark 2. Note that, for $u_h, v_h \in V_{0h}$ with $p \geq 2$, we obtain an alternative representation for the discrete bilinear form

$$\begin{aligned} b_h(u_h, v_h) &= \int_Q (\partial_t u_h v_h + \theta h \partial_t u_h \partial_t v_h + \nabla_x u_h \cdot \nabla_x v_h \\ &\quad + \theta h \nabla_x u_h \cdot \nabla_x \partial_t v_h) dxdt + \theta h \int_{\Sigma} n_t \nabla_x u_h \cdot \nabla_x v_h ds \end{aligned}$$

by integration by parts. For non-moving domains, we observe that $n_t = 0$ on Σ , and we therefore obtain

$$b_h(u_h, v_h) = a_h(u_h, v_h) \quad \text{for all } u_h, v_h \in V_{0h}.$$

Hence, in the case of a non-moving domain, the discrete variational formulation (3.11) is equivalent to the discrete problem (5.2).

In the next lemma, we show that the discrete bilinear form for the moving spatial domain is V_{0h} -coercive wrt to the energy norm

$$\|v\|_{h,m} := \left[\|v\|_h^2 + \theta h \|\nabla_x v\|_{L_2(\Sigma_T)}^2 \right]^{\frac{1}{2}}.$$

Lemma 8. *Let $\theta > 0$ be sufficiently small, in particular, we assume*

$$\theta < (2C_{inv,1}C_u)^{-1},$$

where $C_{inv,1}$ is the constant from Lemma 3 and the constant $C_u > 0$ is given by the quasi uniform assumption (3.7). Then the discrete bilinear form $b_h(\cdot, \cdot) : V_{0h} \times V_{0h} \rightarrow \mathbb{R}$, defined by (5.3), is V_{0h} -coercive wrt the norm $\|\cdot\|_{h,m}$, i.e.

$$b_h(v_h, v_h) \geq \mu_c \|v_h\|_{h,m}^2, \quad \forall v \in V_{0h} \quad (5.4)$$

with $\mu_c = 1/2$.

Proof. Let $v_h \in V_{0h}$. By means of the definition of the discrete bilinear term $b_h(\cdot, \cdot)$ from (5.3) and using Gauss' theorem, we get

$$\begin{aligned} b_h(v_h, v_h) &= \int_Q [\partial_t v_h v_h + \theta h (\partial_t v_h)^2 + \nabla_x v_h \cdot \nabla_x v_h - \theta h \partial_t \nabla_x v_h \cdot \nabla_x v_h] dxdt \\ &\quad + \theta h \int_{\Sigma_T} \nabla_x v_h \cdot \nabla_x v_h ds \\ &= \int_Q \left[\frac{1}{2} \partial_t v_h^2 + \theta h (\partial_t v_h)^2 + |\nabla_x v_h|^2 - \theta h \partial_t \nabla_x v_h \cdot \nabla_x v_h \right] dxdt \\ &\quad + \theta h \int_{\Sigma_T} |\nabla_x v_h|^2 ds \\ &= \frac{1}{2} \int_{\partial Q} v_h^2 n_t ds + \theta h \|\partial_t v_h\|_{L_2(Q)}^2 + \|\nabla_x v_h\|_{L_2(Q)}^2 \\ &\quad - \theta h \int_Q \partial_t \nabla_x v_h \cdot \nabla_x v_h dxdt + \theta h \|\nabla_x v_h\|_{L_2(\Sigma_T)}^2 \end{aligned}$$

for all $v \in V_{0h}$. Since $v_h = 0$ on $\Sigma \cup \Sigma_0$, we further obtain

$$\begin{aligned} b_h(v_h, v_h) &= \frac{1}{2} \|v_h\|_{L_2(\Sigma_T)}^2 + \theta h \|\partial_t v_h\|_{L_2(Q)}^2 + \|\nabla_x v_h\|_{L_2(Q)}^2 + \theta h \|\nabla_x v_h\|_{L_2(\Sigma_T)}^2 \\ &\quad - \theta h \int_Q \partial_t \nabla_x v_h \cdot \nabla_x v_h dxdt \\ &\geq \|v_h\|_{h,m}^2 - \theta h \|\partial_t \nabla_x v_h\|_{L_2(Q)} \|\nabla_x v_h\|_{L_2(Q)} \quad \text{for all } v_h \in V_{0h}. \end{aligned}$$

By using the inverse inequality (4.5) and the assumption (3.7) we further obtain similar to the proof of Lemma 4 the estimate

$$\begin{aligned} \|\partial_t \nabla_x v_h\|_{L_2(Q)}^2 &= \sum_{K \in \mathcal{K}_h} \|\partial_t \nabla_x v_h\|_{L_2(K)}^2 \leq \sum_{K \in \mathcal{K}_h} C_{inv,1}^2 h_K^{-2} \|\nabla_x v_h\|_{L_2(K)}^2 \\ &\leq C_{inv,1}^2 C_u^2 h^{-2} \sum_{K \in \mathcal{K}_h} \|\nabla_x v_h\|_{L_2(K)}^2 = [C_{inv,1} C_u h^{-1} \|\nabla_x v_h\|_{L_2(Q)}]^2. \end{aligned}$$

Hence, we have for $\theta < (2C_{inv,1}C_u)^{-1}$ the estimate for the bilinear form

$$\begin{aligned} b_h(v_h, v_h) &\geq \|v_h\|_{h,m}^2 - \theta h \|\partial_t \nabla_x v_h\|_{L_2(Q)} \|\nabla_x v_h\|_{L_2(Q)} \\ &\geq (1 - \theta h C_{inv,1} C_u h^{-1}) \|v_h\|_{h,m}^2 \geq \frac{1}{2} \|v_h\|_{h,m}^2. \end{aligned}$$

□

To show the boundedness for the bilinear form $b_h(\cdot, \cdot)$, we need the following additional norm

$$\|v\|_{h,m,*} := \left[\|v\|_{h,m} + (\theta h)^{-1} \|v\|_{L_2(Q)}^2 + (\theta^2 h^2) \|\partial_t \nabla_x v\|_{L_2(Q)}^2 \right]^{\frac{1}{2}}.$$

Lemma 9. *The discrete bilinear form $b_h(\cdot, \cdot) : V_{0h,*} \times V_{0h} \rightarrow \mathbb{R}$, defined by (5.3), is uniformly bounded on $V_{0h,*} \times V_{0h}$, i.e., there exists a positive constant μ_b which does not depend on h such that*

$$|b_h(u, v_h)| \leq \mu_b \|u\|_{h,m,*} \|v_h\|_{h,m} \quad (5.5)$$

for all $u \in V_{0h,*}$ and all $v_h \in V_{0h}$.

Proof. We estimate the discrete bilinear form (5.3)

$$\begin{aligned} b_h(u, v_h) &= \int_Q (\partial_t u v_h + \theta h \partial_t u \partial_t v_h + \nabla_x u \cdot \nabla_x v_h - \theta h \partial_t \nabla_x u \cdot \nabla_x v_h) \, dx dt \\ &\quad + \theta h \int_{\Sigma_T} \nabla_x u \cdot \nabla_x v_h \, ds \end{aligned}$$

term by term. For the first, second and third term, we can proceed as in the non-moving case, and we obtain the estimates

$$\begin{aligned} \int_Q \partial_t u v_h \, dx dt &\leq (\theta h)^{-\frac{1}{2}} \|u\|_{L_2(Q)} (\theta h)^{\frac{1}{2}} \|\partial_t v_h\|_{L_2(Q)} \\ &\quad + \|u\|_{L_2(\Sigma_T)} \|v_h\|_{L_2(\Sigma_T)}, \\ \theta h \int_Q \partial_t u \partial_t v_h \, dx dt &\leq (\theta h)^{\frac{1}{2}} \|\partial_t u\|_{L_2(Q)} (\theta h)^{\frac{1}{2}} \|\partial_t v_h\|_{L_2(Q)}, \\ \int_Q \nabla_x u \cdot \nabla_x v_h \, dx dt &\leq \|\nabla_x u\|_{L_2(Q)} \|\nabla_x v_h\|_{L_2(Q)}. \end{aligned}$$

For the two remaining terms, we also use the Cauchy-Schwarz inequality, and we obtain

$$\begin{aligned} \theta h \int_Q \partial_t \nabla_x u \cdot \nabla_x v_h \, dx dt &\leq \theta h \|\partial_t \nabla_x u\|_{L_2(Q)} \|\nabla_x v_h\|_{L_2(Q)}, \\ \theta h \int_{\Sigma_T} \nabla_x u \cdot \nabla_x v_h \, ds &\leq (\theta h)^{\frac{1}{2}} \|\nabla_x u\|_{L_2(\Sigma_T)} (\theta h)^{\frac{1}{2}} \|\nabla_x v_h\|_{L_2(\Sigma_T)}. \end{aligned}$$

Combining these estimates, we conclude the statement of this Lemma with

$$\begin{aligned} b_h(u, v_h) &\leq \left[(\theta h)^{-1} \|u\|_{L_2(Q)}^2 + \|u\|_{L_2(\Sigma_T)}^2 + \theta h \|\partial_t u\|_{L_2(Q)}^2 \right. \\ &\quad \left. + \|\nabla_x u\|_{L_2(Q)}^2 + \theta^2 h^2 \|\partial_t \nabla_x u\|_{L_2(Q)}^2 + \theta h \|\nabla_x u\|_{L_2(\Sigma_T)}^2 \right]^{\frac{1}{2}} \\ &\times \left[\theta h \|\partial_t v_h\|_{L_2(Q)}^2 + \|v_h\|_{L_2(\Sigma_T)}^2 + \theta h \|\partial_t v_h\|_{L_2(Q)}^2 \right. \\ &\quad \left. + \|\nabla_x v_h\|_{L_2(Q)}^2 + \|\nabla_x v_h\|_{L_2(Q)}^2 + \theta h \|\nabla_x v_h\|_{L_2(\Sigma_T)}^2 \right]^{\frac{1}{2}} \\ &\leq 2 \|u\|_{h,m,*} \|v_h\|_{h,m}. \end{aligned}$$

□

Lemma 10. *Let s be a positive integer with $2 \leq s \leq p + 1$, and let $v \in H^s(Q)$. Then there exist a projection Π_h from $H_{0,0}^{1,1}(Q) \cap H^s(Q)$ to V_{0h} , and generic constants $C_1, C_2 > 0$ such that the following error estimates hold*

$$\|v - \Pi_h v\|_{h,m} \leq C_1 h^{s-1} \|v\|_{H^s(Q)}, \quad (5.6)$$

$$\|v - \Pi_h v\|_{h,m,*} \leq C_2 h^{s-1} \|v\|_{H^s(Q)}, \quad (5.7)$$

where p denotes the underlying polynomial degree of the B-spline resp. NURBS.

Proof. By using Lemma 6 it remains to estimate the additional terms

$$h^2 \|\partial_t \nabla_x (v - \Pi_h v)\|_{L_2(Q)}^2 \quad \text{and} \quad h \|\nabla_x (v - \Pi_h v)\|_{L_2(\Sigma_T)}^2.$$

With Lemma 5 we obtain for $i, j = 1, \dots, d + 1$

$$\|\partial_{x_i} \partial_{x_j} (v - \Pi_h v)\|_{L_2(Q)} \leq C_s h^{s-2} \|v\|_{H^s(Q)}. \quad (5.8)$$

By using the error estimate (5.8) we obtain

$$\begin{aligned} h^2 \|\partial_t \nabla_x (v - \Pi_h v)\|_{L_2(Q)}^2 &= h^2 \sum_{i=1}^d \|\partial_t \partial_{x_i} (v - \Pi_h v)\|_{L_2(Q)}^2 \\ &\leq h^2 \sum_{i=1}^d C_s^2 h^{2(s-2)} \|v\|_{H^s(Q)}^2 \\ &= \left[\sqrt{d} C_s h^{s-1} \|v\|_{H^s(Q)} \right]^2. \end{aligned}$$

With Lemma 2 and using also (5.8) we further obtain

$$\begin{aligned} h \|\nabla_x (v - \Pi_h v)\|_{L_2(\Sigma_T)}^2 &= h \sum_{\substack{K \in \mathcal{K}_h \\ \partial K \cap \Sigma_T \neq \emptyset}} \sum_{i=1}^d \|\partial_{x_i} (v - \Pi_h v)\|_{L_2(\partial K \cap \Sigma_T)}^2 \\ &\leq h \sum_{\substack{K \in \mathcal{K}_h \\ \partial K \cap \Sigma_T \neq \emptyset}} \sum_{i=1}^d C_{tr}^2 h_K^{-1} \left(\|\partial_{x_i} (v - \Pi_h v)\|_{L_2(K)} + h_K |\partial_{x_i} (v - \Pi_h v)|_{H^1(K)} \right)^2 \\ &\leq 2C_u C_{tr}^2 \sum_{\substack{K \in \mathcal{K}_h \\ \partial K \cap \Sigma_T \neq \emptyset}} \sum_{i=1}^d \left(\|\partial_{x_i} (v - \Pi_h v)\|_{L_2(K)}^2 + h^2 |\partial_{x_i} (v - \Pi_h v)|_{H^1(K)}^2 \right) \\ &\leq 2C_u C_{tr}^2 \left[\|\nabla_x (v - \Pi_h v)\|_{L_2(Q)}^2 + h^2 \sum_{i=1}^d |\partial_{x_i} (v - \Pi_h v)|_{H^1(Q)}^2 \right] \\ &= 2C_u C_{tr}^2 \left[\|\nabla_x (v - \Pi_h v)\|_{L_2(Q)}^2 + h^2 \sum_{i=1}^d \sum_{j=1}^{d+1} |\partial_{x_i} \partial_{x_j} (v - \Pi_h v)|_{H^1(Q)}^2 \right] \\ &\leq \left[\sqrt{2(1+d(d+1))} C_u C_{tr} C_s h^{s-1} \|v\|_{H^s(Q)} \right]^2, \end{aligned}$$

which completes the proof. \square

Lemma 11. *Let $p \geq 2$. If the solution $u \in H_0^{1,0}(Q)$ of the variational problem (2.1) belongs to $H^2(Q)$, then it satisfies the consistency identity*

$$b_h(u, v_h) = l_h(v_h) \quad \forall v_h \in V_{0h}.$$

Proof. With the same arguments as in Lemma 7, we obtain that

$$\partial_t u - \Delta u = f \quad \text{in } L_2(Q) \quad \text{and} \quad u = u_0 \quad \text{in } L_2(\Sigma_0). \quad (5.9)$$

We now multiply the differential equation of (5.9) with a test function $v_h + \theta h \partial_t v_h$ for $v_h \in V_{0h}$ and integrate over the space-time domain Q . Since $u \in H^2(Q)$ and $p \geq 2$, we can apply all the derivations as we did at the beginning of this section to obtain the statement of this Lemma. \square

Theorem 2. *Let $p \geq 2$ and θ be sufficiently small, see Lemma 8. Furthermore, let $u \in H_0^{1,0}(Q) \cap H^s(Q)$ with $s \geq 2$ be the exact solution of the model problem (2.1), and let $u_h \in V_{0h}$ be the solution to discrete variational problem (5.2). Then the discretization error estimate*

$$\|u - u_h\|_{h,m} \leq Ch^{t-1} \|u\|_{H^t(Q)}, \quad (5.10)$$

holds, where $t = \min\{s, p + 1\}$, and p denotes the underlying polynomial degree of the NURBS.

Proof. The stated error estimate follows in the exact way as in Theorem 1 by using Lemma 8–11. \square

Remark 3. For the case $p = 1$, Lemma 11 is not valid in general. In this case, we have to take additional consistency errors into account by estimating them properly. It turns out, cf. Subsection 6.2, that also, for the case $p = 1$, we obtain the full convergence rates wrt the energy norm $\|\cdot\|_{h,m}$ for smooth solutions.

6 Numerical Results

The numerical results presented below have been performed in **G+SMO**¹ [24]. We used the sparse direct solver SuperLU to solve the resulting linear system (3.16) of IgA equations. We present numerical results for both fixed (Subsection 6.1) and moving (Subsection 6.2) spatial computational domains in one and two dimensions in space. In Subsection 6.3, we present numerical results which demonstrate the efficiency of a standard parallel AMG preconditioned GMRES solver on massively parallel computers with several thousands of cores. We mention that θ was set to 0.1 in all our numerical experiments including the examples with moving spatial domains.

6.1 Fixed Spatial Computational Domain

¹ *Geometry plus Simulation Modules*, <http://www.gs.jku.at/gismo>

6.1.1 Fixed one-dimensional spatial computational domain. We consider the one-dimensional spatial domain $\Omega = (0, 1)$ and the time interval $(0, T)$ with $T = 1$, i.e., we have the space-time cylinder $Q = (0, 1)^2$, that can geometrically be represented by the knot vectors $\Xi_1 = \{0, 0, 1, 1\}$ and $\Xi_2 = \{0, 0, 1, 1\}$ in the IgA context. We solve our parabolic boundary value problem (1.1), and choose the data such that the solution is given by $u(x_1, t) = u(x, t) = \sin(\pi x) \sin(\pi t)$, i.e. $f(x, t) = \partial_t u(x, t) - \Delta u(x, t) = \pi \sin(\pi x)(\cos(\pi t) + \pi \sin(\pi t))$ in Q , $u_0 = 0$ on $\overline{\Omega}$, and u obviously vanishes on Σ . Thus, the compatibility condition between boundary and initial conditions holds. The convergence behavior of the space-time IgA scheme with respect to the discrete norm $\|\cdot\|_h$ is shown in Tables 1 and 2 by a series of h -refinement and by using B-splines of polynomial degrees $p = 1, 2, 3, 4$. After some saturation, we observe the optimal convergence rate $O(h^p)$ as theoretically predicted by Theorem 1 for smooth solutions. Moreover, Tables 3 and 4 show the L_2 errors and the corresponding rates for the same setting. We see that the L_2 rates are asymptotically optimal as well, i.e. the L_2 -error behaves like $O(h^{p+1})$.

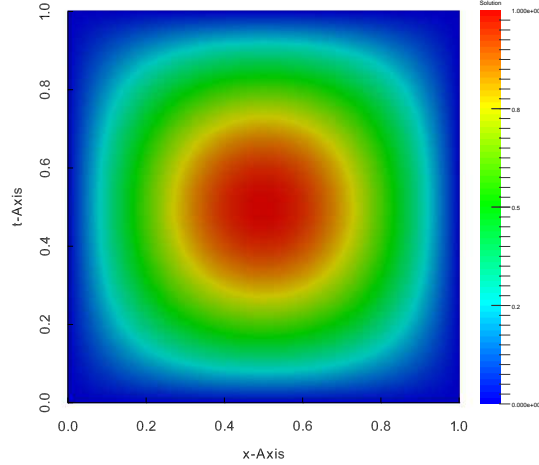


Fig. 3. Solution contours in the space-time cylinder Q for Example 6.1.1.

p = 1			p = 2		
Dofs	$\ u - u_h\ _h$	Rate	Dofs	$\ u - u_h\ _h$	Rate
4	1.6782e+00	0	9	2.10399e-01	0
9	7.28214e-01	1.20	16	2.03729e-01	0.04
25	3.61278e-01	1.01	36	3.98228e-02	2.35
81	1.79489e-01	1.01	100	9.29436e-03	2.10
289	8.94084e-01	1.01	324	2.27848e-03	2.02
1089	4.46132e-02	1.00	1156	5.66197e-04	2.01
4225	2.22829e-02	1.00	4356	1.41258e-04	2.00
16641	1.11354e-02	1.00	16900	3.52865e-05	2.00

Table 1. Errors and rates wrt $\|\cdot\|_h$ for Example 6.1.1 and degrees $p = 1$ and $p = 2$.

p = 3			p = 4		
Dofs	$\ u - u_h\ _h$	Rate	Dofs	$\ u - u_h\ _h$	Rate
16	2.10106e-01	0	25	6.70957e-03	0
25	2.73234e-02	2.92	36	6.49630e-03	0.05
49	5.08124e-03	2.43	64	5.56376e-04	3.55
121	5.73528e-04	3.15	144	3.27142e-05	4.10
361	6.93807e-05	3.05	400	2.05481e-06	4.00
1225	8.58843e-06	3.01	1296	1.30057e-07	4.00
4489	1.07029e-06	3.00	4624	8.20252e-09	4.00
17161	1.33647e-07	3.00	17424	5.15378e-10	4.00

Table 2. Errors and rates wrt $\|\cdot\|_h$ for Example 6.1.1 and degrees $p = 3$ and $p = 4$.

p = 1			p = 2		
Dofs	$\ u - u_h\ _{L_2(Q)}$	Rate	Dofs	$\ u - u_h\ _{L_2(Q)}$	Rate
4	5.000e-01	0	9	2.69186e-02	0
9	1.21333e-01	2.04	16	2.66817e-02	0.03
25	3.03720e-02	2.00	36	2.30767e-03	3.53
81	7.47639e-03	2.02	100	2.60187e-04	3.15
289	1.85552e-03	2.01	324	3.16609e-05	3.04
1089	4.62271e-04	2.00	1156	3.92785e-06	3.01
4225	1.15377e-04	2.00	4356	4.89712e-07	3.01
16641	2.88212e-05	2.00	16900	6.11484e-08	3.00

Table 3. L_2 errors and rates for Example 6.1.1 using degrees $p = 1$ and $p = 2$.

6.1.2 Fixed two-dimensional spatial computational domain. As a second example we consider the two-dimensional spatial domain $\Omega = (0, 1)^2$ and the time interval $(0, T)$ with $T = 1$, i.e., we have the space-time cylinder $Q = (0, 1)^3$, that can geometrically be represented by the knot

p = 3			p = 4		
Dofs	$\ u - u_h\ _{L_2(Q)}$	Rate	Dofs	$\ u - u_h\ _{L_2(Q)}$	Rate
16	2.65068e-02	0	25	5.49027e-04	0
25	2.32514e-03	3.16	36	5.43598e-04	0.01
49	3.10354e-04	2.84	64	3.90240e-05	3.80
121	1.63884e-05	4.25	144	1.02403e-06	5.25
361	9.72892e-07	4.10	400	3.03989e-08	5.07
1225	5.99946e-08	4.02	1296	9.38131e-10	5.02
4489	3.73705e-09	4.01	4624	2.92231e-11	5.00
17161	2.33370e-10	4.00	17424	9.15973e-13	5.00

Table 4. L_2 errors and rates for Example 6.1.1 using degrees $p = 3$ and $p = 4$.

vectors $\Xi_1 = \{0, 0, 1, 1\}$, $\Xi_2 = \{0, 0, 1, 1\}$ and $\Xi_3 = \{0, 0, 1, 1\}$ in the context of IgA. We solve our model problem (1.1), and again choose the data such that the solution is given by $u(x, t) = \sin(\pi x_1) \sin(\pi x_2) \sin(\pi t)$, i.e. $f(x, t) = \partial_t u(x, t) - \Delta u(x, t) = \pi \sin(\pi x_1) \sin(\pi x_2) (\cos(\pi t) + 2\pi \sin(\pi t))$ in Q , $u_0 = 0$ on $\overline{\Omega}$, and u obviously vanishes on Σ . Thus, the compatibility condition between boundary and initial conditions holds. In Figure 4, we present the solution contours of the problem in \mathbb{R}^3 , where we have sliced the domain along the t -axis. The convergence behavior of the space-time IgA scheme with respect to the discrete norm $\|\cdot\|_h$ is shown in Tables 5 and 6 by a series of h -refinement and by using B-splines of polynomial degrees $p = 1, 2, 3, 4$. After some saturation, we observe the optimal convergence rate $O(h^p)$ as theoretically predicted by Theorem 1 for smooth solutions. Moreover, Tables 7 and 8 show the L_2 errors and the corresponding rates for the same setting. We see that the L_2 rates are asymptotically optimal as well, i.e. the L_2 -error behaves like $O(h^{p+1})$.

p = 1			p = 2		
Dofs	$\ u - u_h\ _h$	Rate	Dofs	$\ u - u_h\ _h$	Rate
8	1.63740	0	27	2.15440e-01	0
27	7.39981e-01	1.15	64	2.11247e-01	0.03
125	3.60495e-01	1.04	216	3.98871e-02	2.40
729	1.79065e-01	1.01	1000	9.27926e-03	2.10
4913	8.92787e-02	1.00	5832	2.27556e-03	2.03
35937	4.45779e-02	1.00	39304	5.65772e-04	2.01

Table 5. Errors and rates wrt $\|\cdot\|_h$ for Example 6.1.2 and degrees $p = 1$ and $p = 2$.

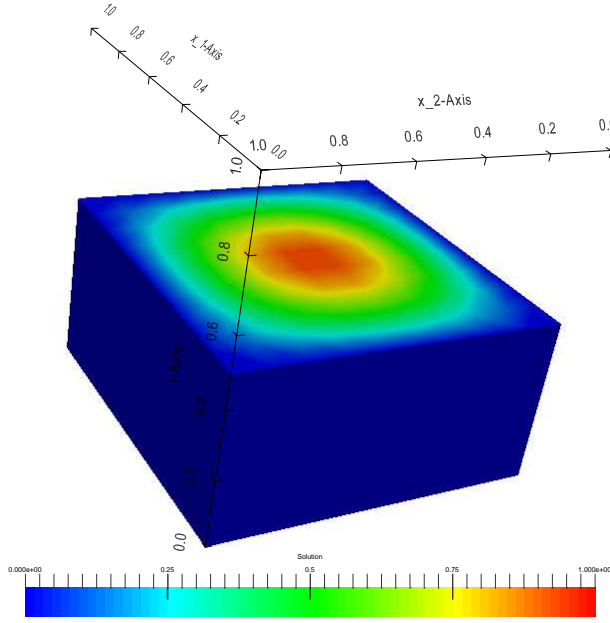


Fig. 4. Solution contours in the space-time cylinder Q at $t = 0.5$ for Example 6.1.2.

p = 3			p = 4		
Dofs	$\ u - u_h\ _h$	Rate	Dofs	$\ u - u_h\ _h$	Rate
64	2.16883e-01	0	125	6.67416e-03	0
125	2.75120e-02	2.97	216	7.69213e-03	0.03
343	5.09465e-03	2.43	512	3.55820e-03	3.55
1331	5.72742e-04	3.15	1728	3.26623e-05	4.10
6859	6.92964e-05	3.04	8000	2.05215e-06	4.00
42875	8.58214e-06	3.01	46656	1.37611e-07	4.00

Table 6. Errors and rates wrt $\|\cdot\|_h$ for Example 6.1.2 and degrees $p = 3$ and $p = 4$.

6.2 Moving Spatial Computational Domain

6.2.1 A simple one-dimensional moving spatial computational domain. Now we consider the one-dimensional moving computational domain $\Omega(t) = \{x = x_1 \in \mathbb{R}^1 : a(t) < x < b(t)\}$ with $t \in (0, T)$, where $a(t) = -t/2$, $b(t) = 1 + t/2$, and $T = 1$. The space-time cylinder $Q = \{(x, t) \in \mathbb{R}^2 : x \in \Omega(t), t \in (0, T)\} \subset \mathbb{R}^2$ is obviously a fixed domain

p = 1			p = 2		
Dofs	$\ u - u_h\ _{L_2(Q)}$	Rate	Dofs	$\ u - u_h\ _{L_2(Q)}$	Rate
8	3.65528e-01	0	27	2.39153e-02	0
27	9.56396e-02	1.93	64	2.37388e-02	0.01
125	2.32679e-02	2.03	216	1.99848e-03	3.57
729	5.75358e-03	2.01	1000	2.22710e-04	3.17
4913	1.43171e-03	2.01	5832	2.70486e-05	3.04
35937	3.57195e-04	2.00	39304	3.35780e-06	3.00

Table 7. L_2 errors and rates for Example 6.1.2 using degree $p = 1$ and $p = 2$.

p = 3			p = 4		
Dofs	$\ u - u_h\ _{L_2(Q)}$	Rate	Dofs	$\ u - u_h\ _{L_2(Q)}$	Rate
64	2.39325e-02	0	125	4.75391e-04	0
125	2.03108e-03	3.56	216	4.73425e-04	0.01
343	2.68174e-04	2.92	512	3.34666e-05	3.82
1331	1.41715e-05	4.24	1728	8.74291e-07	5.26
6859	8.42223e-07	4.07	8000	2.60544e-08	5.07
42875	5.19528e-08	4.01	46656	8.07120e-10	5.01

Table 8. L_2 errors and rates for Example 6.1.2 using degree $p = 3$ and $p = 4$.

in the space-time world \mathbb{R}^2 . It can geometrically be represented by the knot vectors $\Xi_1 = \{0, 0, 1, 1\}$ and $\Xi_2 = \{0, 0, 1, 1\}$ and the control points $\mathbf{P}_{1,1} = (0, 0)$, $\mathbf{P}_{2,1} = (1, 0)$, $\mathbf{P}_{2,2} = (1.5, 1.0)$, and $\mathbf{P}_{1,2} = (-0.5, 1.0)$ in the context of IgA. We solve our model problem (1.1), and again choose the data such that the solution is given by $u(x, t) = \sin(\pi x) \sin(\pi t)$, i.e. $f(x, t) = \partial_t u(x, t) - \Delta u(x, t) = (\pi \sin(\pi x))(\cos(\pi t) + \pi \sin(\pi t))$ in Q , $u_0 = 0$ on $\overline{\Omega}$, and $u(x, t) = \sin(\pi x) \sin(\pi t)$ on Σ . Thus, the compatibility condition between boundary and initial conditions holds. The space-time computational domain Q and the solution is drawn in Figure 5. The convergence behavior of the space-time IgA scheme with respect to the discrete norm $\|\cdot\|_{h,m}$ is shown in Tables 9 and 10 by a series of h -refinement and by using B-splines of polynomial degrees $p = 1, 2, 3, 4$. After some saturation, we observe the optimal convergence rate $O(h^p)$ for $p \geq 2$ as theoretically predicted by Theorem 2 for smooth solutions. Moreover, Tables 7 and 8 show the L_2 errors and the corresponding rates for the same setting. We see that the L_2 rates are asymptotically optimal for $p \geq 2$ as well, i.e. they behave like $O(h^{p+1})$. For $p = 1$, we also observe the optimal rate in the discrete norm, cf. also Remark 3, whereas the L_2 -rate does not reach the optimal order 2.

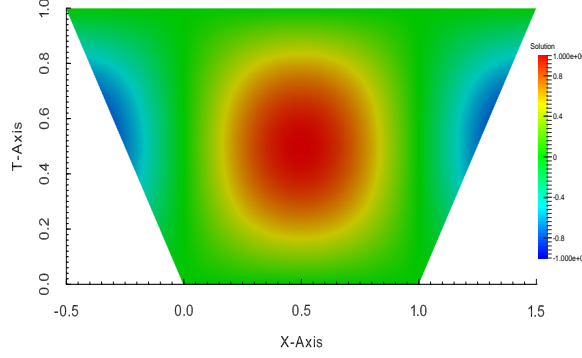


Fig. 5. Solution contours in the space-time cylinder Q for Example 6.2.1.

p = 1			p = 2		
Dofs	$\ u - u_h\ _{h,m}$	Rate	Dofs	$\ u - u_h\ _{h,m}$	Rate
4	2.31256	0	9	8.3047e-01	0
9	8.7222e-01	1.41	16	7.4075e-01	0.17
25	5.9385e-01	0.55	36	1.3091e-01	2.50
81	3.0387e-01	0.97	100	2.9977e-02	2.13
289	1.5240e-01	1.00	324	7.2872e-03	2.04
1089	7.6181e-02	1.00	1156	1.8068e-03	2.01
4225	3.8070e-02	1.00	4356	4.5056e-04	2.00
16641	1.9028e-02	1.00	16900	1.1255e-04	2.00

Table 9. Errors and rates wrt $\|\cdot\|_{h,m}$ for Example 6.2.1 and degrees $p = 1$ and $p = 2$.

6.2.2 Curvilinearly moving one-dimensional spatial computational domain. We consider again an one-dimensional moving spatial computational domain of the form $\Omega(t) = \{x = x_1 \in \mathbb{R}^1 : a(t) < x < b(t)\}$, $t \in (0, 1)$, where now the movement is described by the functions $a(t) = t(1-t)/2$ and $b(t) = 1 - t(1-t)/2$ leading to the space-time cylinder $Q = \{(x, t) \in \mathbb{R}^2 : x \in \Omega(t), t \in (0, T)\} \subset \mathbb{R}^2$ with a curved surface area Σ , see Figure 6. The space-time cylinder Q can also be represented by the knot vectors $\Xi_1 = \{0, 0, 1, 1\}$ and $\Xi_2 = \{0, 0, 0, 1, 1, 1\}$ and the corresponding control points $\mathbf{P}_{1,1} = (0, 0)$, $\mathbf{P}_{2,1} = (1, 0)$, $\mathbf{P}_{2,2} = (0.75, 0.5)$, $\mathbf{P}_{2,3} = (1, 1)$, $\mathbf{P}_{1,3} = (0, 1)$ and $\mathbf{P}_{1,2} = (0.25, 0.5)$ in the context of IgA,

p = 3			p = 4		
Dofs	$\ u - u_h\ _{h,m}$	Rate	Dofs	$\ u - u_h\ _{h,m}$	Rate
16	7.87827e-01	0	25	9.58143e-02	0
25	7.74683e-02	3.35	36	7.29388e-02	0.35
49	2.68888e-02	1.53	64	7.25760e-03	3.31
121	2.54304e-03	3.40	144	3.25434e-04	4.48
361	2.97843e-04	3.09	400	1.83582e-05	4.15
1225	3.69216e-05	3.01	1296	1.11825e-06	4.04
4489	4.62600e-06	3.00	4624	6.95208e-08	4.01
17161	5.79880e-07	3.00	17424	4.34224e-09	4.00

Table 10. Errors and rates wrt $\|\cdot\|_{h,m}$ for Example 6.2.1 using degree $p = 3$ and $p = 4$.

p = 1			p = 2		
Dofs	$\ u - u_h\ _{L_2(Q)}$	Rate	Dofs	$\ u - u_h\ _{L_2(Q)}$	Rate
4	8.7462	0	9	1.9450e-01	0
9	1.9970e-01	2.13	16	1.41565e-01	0.46
25	7.3226e-02	1.45	36	1.09044e-02	3.70
81	1.8794e-02	1.96	100	1.12045e-03	3.28
289	5.0344e-03	1.90	324	1.31179e-04	3.09
1089	1.5998e-03	1.65	1156	1.60564e-05	3.03
4225	6.4746e-04	1.31	4356	1.99240e-06	3.01
16641	3.0437e-04	1.10	16900	2.48337e-07	3.00

Table 11. L_2 errors and rates for Example 6.2.1 using degree $p = 1$ and $p = 2$.

p = 3			p = 4		
Dofs	$\ u - u_h\ _{L_2(Q)}$	Rate	Dofs	$\ u - u_h\ _{L_2(Q)}$	Rate
16	1.69684e-01	0	25	1.38383e-02	0
25	1.02458e-02	4.05	36	1.01827e-02	0.44
49	2.34449e-03	2.13	64	6.76183e-04	3.91
121	9.90173e-05	4.57	144	1.2387e-05	5.77
361	5.56308e-06	4.15	400	3.23506e-07	5.26
1225	3.40489e-07	4.03	1296	9.61797e-09	5.07
4489	2.12529e-08	4.00	4624	2.96841e-10	5.02
17161	1.33061e-09	4.00	17424	9.24929e-12	5.00

Table 12. L_2 errors and rates for Example 6.2.1 using degree $p = 3$ and $p = 4$.

see also Figure 6. We solve our model problem (1.1), and again choose the data such that the solution is given by $u(x, t) = \sin(\pi x) \sin(\pi t)$, i.e. $f(x, t) = \partial_t u(x, t) - \Delta u(x, t) = (\pi \sin(\pi x))(\cos(\pi t) + \pi \sin(\pi t))$ in Q , $u_0 = 0$ on $\bar{\Omega}$, and $u(x, t) = \sin(\pi x) \sin(\pi t)$ on Σ . Thus, the compatibility

condition between boundary and initial conditions hold. The convergence behavior of the space-time IgA scheme with respect to the discrete norm $\|\cdot\|_{h,m}$ is shown in Tables 13 and 14 by a series of h -refinement and by using B-splines of polynomial degrees $p = 1, 2, 3, 4$. After some saturation, we observe the optimal convergence rate $O(h^p)$ for $p \geq 2$ as theoretically predicted by Theorem 2 for smooth solutions. Moreover, Tables 15 and 16 show the L_2 errors and the corresponding rates for the same setting. We see that the L_2 rates are asymptotically optimal for $p \geq 2$ as well, i.e. they behave like $O(h^{p+1})$. For $p = 1$, we also observe the optimal rate in the discrete norm, cf. also Remark 3, whereas the L_2 -rate does not reach the optimal order 2.

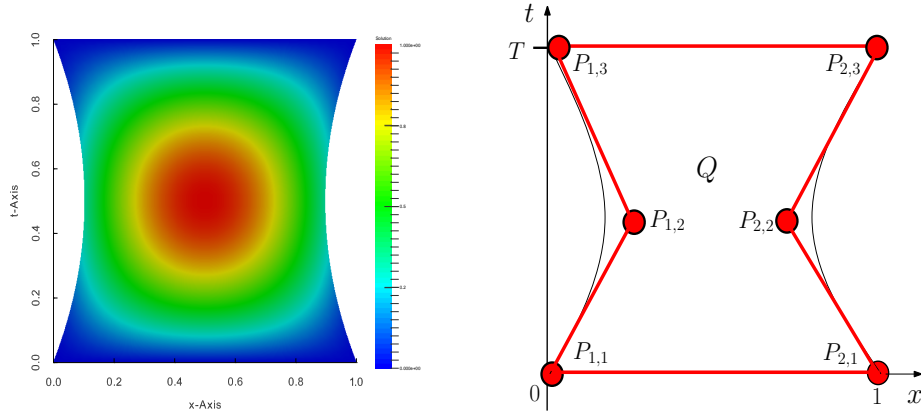


Fig. 6. Solution contours for Example 6.2.2 (left) and the control points (right).

6.2.3 Curvilinearly moving two-dimensional spatial computational domain. We now consider the curvilinearly moving two-dimensional spatial computational domain $\Omega(t) = \{x = (x_1, x_2) \in \mathbb{R}^2 : a(t) < x_1 < b(t), 0 < x_2 < 1\}$ in \mathbb{R}^2 , where $a(t) = t(1-t)/2$, $b(t) = 1 - t(1-t)/2$, and t is running from 0 to $T = 1$, leading to the space-time cylinder $Q = \{(x, t) \in \mathbb{R}^3 : x \in \Omega(t), t \in (0, T)\} \subset \mathbb{R}^3$ that is fixed in the space-time world \mathbb{R}^3 . In the context of IgA, Q can geometrically be represented by the knot vectors $\Xi_1 = \{0, 0, 1, 1\}$, $\Xi_2 = \{0, 0, 1, 1\}$ and $\Xi_3 = \{0, 0, 0, 1, 1, 1\}$, and the control points given in Figure 7 (right). We solve our model problem (1.1), and again choose the data such that

p = 1			p = 2		
Dofs	$\ u - u_h\ _{h,m}$	Rate	Dofs	$\ u - u_h\ _{h,m}$	Rate
4	1.40608e+00	0	9	1.79646e-01	0
9	6.28191e-01	1.15	16	1.66950e-01	0.11
25	3.02013e-01	1.05	36	2.52637e-02	2.72
81	1.47951e-01	1.02	100	5.45976e-03	2.21
289	7.33135e-02	1.01	324	1.29401e-03	2.08
1089	3.65079e-02	1.01	1156	3.16214e-04	2.03
4225	1.82188e-02	1.00	4356	7.82250e-05	2.02
16641	9.10085e-03	1.00	16900	1.94575e-05	2.01

Table 13. Errors and rates wrt $\|\cdot\|_{h,m}$ for Example 6.2.2 and degrees $p = 1$ and $p = 2$.

p = 3			p = 4		
Dofs	$\ u - u_h\ _{h,m}$	Rate	Dofs	$\ u - u_h\ _{h,m}$	Rate
16	2.25659e-01	0	25	1.55287e-02	0
25	1.95569e-02	3.18	36	9.35760e-03	0.73
49	3.37111e-02	2.56	64	3.74209e-04	4.64
121	3.37580e-03	3.25	144	1.93936e-05	4.27
361	3.95998e-04	3.09	400	9.83348e-07	4.30
1225	4.83941e-06	3.03	1296	5.54882e-08	4.14
4489	5.99023e-07	3.01	4624	3.30365e-09	4.07
17161	7.45335e-08	3.01	17424	2.01770e-10	4.03

Table 14. Errors and rates wrt $\|\cdot\|_{h,m}$ for Example 6.2.2 using degree $p = 3$ and $p = 4$.

p = 1			p = 2		
Dofs	$\ u - u_h\ _{L_2(Q)}$	Rate	Dofs	$\ u - u_h\ _{L_2(Q)}$	Rate
4	4.03831e-01	0	9	2.93862e-02	0
9	9.12333e-02	2.14	16	3.21213e-02	0.13
25	2.33973e-02	1.96	36	2.74769e-03	3.55
81	5.79121e-03	2.01	100	3.10332e-04	3.15
289	1.52473e-03	1.92	324	3.77756e-05	3.03
1089	4.68079e-04	1.70	1156	4.68649e-06	3.01
4290	1.82024e-04	1.36	4356	5.84132e-07	3.00
16770	8.37613e-05	1.12	16900	7.29169e-08	3.00

Table 15. L_2 errors and rates for Example 6.2.2 using degree $p = 1$ and $p = 2$.

the solution is given by $u(x, t) = \sin(\pi x_1) \sin(\pi x_2) \sin(\pi t)$, i.e. $f(x, t) = \partial_t u(x, t) - \Delta u(x, t) = (\pi \sin(\pi x_1) \sin(\pi x_2))(\cos(\pi t) + 2\pi \sin(\pi t))$ in Q , $u_0 = 0$ on $\bar{\Omega}$, and $u(x, t) = \sin(\pi x_1) \sin(\pi x_2) \sin(\pi t)$ on Σ . In Figure 7 (left), we present the solution contours of the problem in \mathbb{R}^3 at $t = 0.5$.

p = 3			p = 4		
Dofs	$\ u - u_h\ _{L_2(Q)}$	Rate	Dofs	$\ u - u_h\ _{L_2(Q)}$	Rate
16	3.22870e-02	0	25	1.00347e-03	0
25	2.61893e-03	3.62	36	9.49495e-04	0.10
49	4.05805e-04	2.69	64	5.65065e-05	4.10
121	1.99434e-05	4.34	144	1.96066e-06	4.85
361	1.15336e-06	4.11	400	6.03483e-08	5.02
1225	7.10583e-08	4.02	1296	1.88123e-09	5.00
4489	4.43879e-09	4.00	4624	5.88213e-11	5.00
17161	2.77796e-10	4.00	17424	1.83916e-12	5.00

Table 16. L_2 errors and rates for Example 6.2.2 using degree $p = 3$ and $p = 4$.

The convergence behavior of the space-time IgA scheme with respect to the discrete norm $\|\cdot\|_{h,m}$ is shown in Tables 17 and 18 by a series of h -refinement and by using B-splines of polynomial degrees $p = 1, 2, 3, 4$. After some saturation, we observe the optimal convergence rate $O(h^p)$ for $p \geq 2$ as theoretically predicted by Theorem 2 for smooth solutions. Moreover, Tables 19 and 20 show the L_2 errors and the corresponding rates for the same setting. We see that the L_2 rates are asymptotically optimal for $p \geq 2$ as well, i.e. they behave like $O(h^{p+1})$. For $p = 1$, we also observe the optimal rate in the discrete norm, cf. also Remark 3, whereas the L_2 -rate does not reach the optimal order 2.

p = 1			p = 2		
Dofs	$\ u - u_h\ _{h,m}$	Rate	Dofs	$\ u - u_h\ _{h,m}$	Rate
8	1.57742e+00	0	27	2.5829e-01	0
27	6.84322e-01	1.20	64	2.0891e-01	0.31
125	3.25869e-01	1.07	216	3.64503e-02	2.52
729	1.60291e-01	1.02	1000	7.88416e-03	2.21
4913	7.96709e-02	1.01	5832	1.85329e-03	2.08
35937	3.97383e-02	1.00	39304	4.50536e-04	2.04

Table 17. Errors and rates wrt $\|\cdot\|_{h,m}$ for Example 6.2.3 using degree $p = 1$ and $p = 2$.

6.3 Parallel Solution for the Case $p = 1$

We here consider exactly the same problem as in Subsection 6.1.2, i.e., our parabolic model problem is posed in the 3d space-time domain $Q = (0, 1)^3$. For simplicity, we here consider only the case $p = 1$ that turns

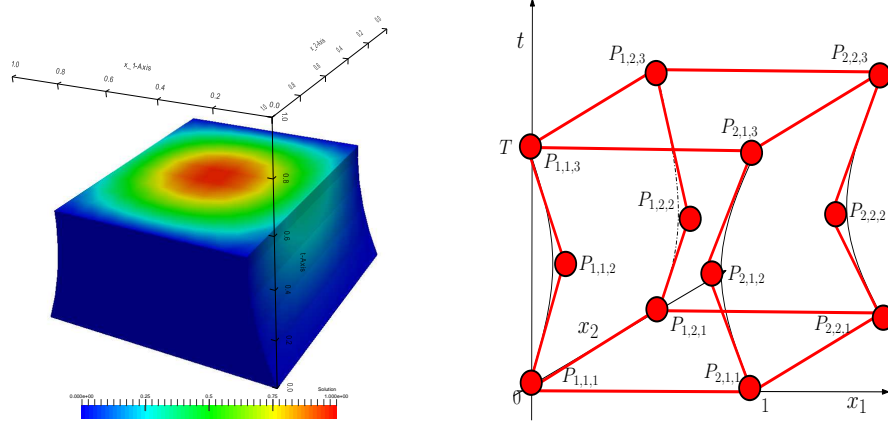


Fig. 7. Solution contours for Example 6.2.3 (left) and the control points (right) are given by $\mathbf{P}_{i_1, i_2, i_3} = \{ (0, 0, 0), (1, 0, 0), (0, 1, 0), (1, 1, 0), (0.25, 0, 0.50), (0.75, 0, 0.5), (0.25, 1, 0.5), (0.75, 1, 0.5), (0, 0, 1), (1, 0, 1), (0, 1, 1), (1, 1, 1) \}$ for $i_1 = 1, 2, i_2 = 1, 2$ and $i_3 = 1, 2, 3$.

p = 3			p = 4		
Dofs	$\ u - u_h\ _{h,m}$	Rate	Dofs	$\ u - u_h\ _{h,m}$	Rate
64	2.41099e-01	0	125	9.93223e-03	0
125	2.65597e-02	3.18	216	7.60959e-03	0.38
343	4.25800e-03	2.64	512	4.70558e-04	4.02
1331	4.58251e-04	3.21	1728	2.72696e-05	4.11
6859	5.46583e-05	3.06	8000	1.60187e-06	4.09
42875	6.73180e-06	3.02	42875	9.81655e-08	4.03

Table 18. Errors and rates wrt $\|\cdot\|_{h,m}$ for Example 6.2.3 using degrees $p = 3$ and $p = 4$.

p = 1			p = 2		
Dofs	$\ u - u_h\ _{L_2(Q)}$	Rate	Dofs	$\ u - u_h\ _{L_2(Q)}$	Rate
8	3.37961e-01	0	27	2.67611e-02	0
27	7.67535e-02	2.14	64	2.66302e-02	0.01
125	1.95993e-02	1.96	216	2.33938e-03	3.51
729	4.86526e-03	2.01	1000	2.63360e-04	3.15
4913	1.25329e-03	1.95	5832	3.20369e-05	3.04
35937	3.61179e-04	1.79	39304	3.97751e-06	3.00

Table 19. L_2 errors and rates for Example 6.2.3 using degrees $p = 1$ and $p = 2$.

p = 3			p = 4		
Dofs	$\ u - u_h\ _{L_2(Q)}$	Rate	Dofs	$\ u - u_h\ _{L_2(Q)}$	Rate
64	2.65683e-01	0	125	6.83584e-04	0
125	2.26323e-03	3.55	216	6.75251e-04	0.02
343	3.36653e-04	2.74	512	3.96777e-05	4.09
1331	1.70973e-05	4.30	1728	1.60770e-06	4.63
6859	9.93566e-07	4.10	8000	5.11255e-08	4.97
42875	6.12843e-08	4.02	46656	1.61035e-09	4.99

Table 20. L_2 errors and rates for Example 6.2.3 using degrees $p = 3$ and $p = 4$.

out to be the finite element case with trilinear hexahedral finite elements. First, we decompose the space-time mesh into several subdomains and assemble the arising linear systems of Subsection 6.1.2 in parallel. For example, in Figure 8, the space-time decomposition with 64 subdomains is shown. Afterwards, we solve these linear systems also in parallel with the GMRES method, where we apply the AMG library hypre as a preconditioner. For the stopping criteria, we use the relative residual error reduction by 10^{-10} . In Table 21, we show the iteration numbers and the solving times for different uniform refinement levels, where we increase the number of cores for larger problems. We observe that the iteration numbers are slightly increasing, but the performance of this solver is still very good, even if this solver was not constructed for space-time problems. This example was computed on the supercomputer Vulcan BlueGene/Q in Livermore, California U.S.A by using the finite element library MFEM.

Dofs	$\ u - u_h\ _{L_2(Q)}$	Rate	iter	time [s]	cores
8	3.65528e-01	-	1	0.01	1
27	9.39008e-02	1.961	2	0.01	1
125	2.32674e-02	2.013	6	0.01	1
729	5.75635e-03	2.015	15	0.07	64
4 913	1.43198e-03	2.007	16	0.14	64
35 937	3.57217e-04	2.003	19	0.40	64
274 625	8.92171e-05	2.001	24	1.04	1 024
2 146 689	2.22941e-05	2.001	29	3.65	1 024
16 974 593	5.57231e-06	2.000	36	21.40	1 024
135 005 697	1.39293e-06	2.000	50	36.26	8 192
1 076 890 625	3.48206e-07	2.000	63	156.50	16 384

Table 21. Solver performance for Example 6.1.2 and $p = 1$.

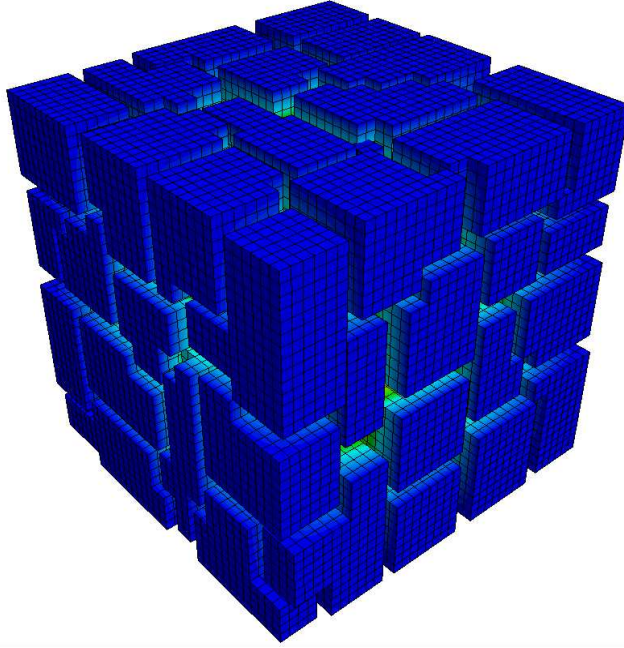


Fig. 8. Space-time decomposition with 64 subdomains.

7 Conclusions

We have introduced the Space-Time IgA for parabolic evolution problems. We have presented a-priori error estimates and numerical examples in the space-time domain $Q = \{(x, t) \in \mathbb{R}^{d+1} : x \in \Omega(t), t \in (0, T)\}$ for both fixed spatial domains $\Omega \subset \mathbb{R}^d$ and moving spatial domains $\Omega(t) \subset \mathbb{R}^d$, $t \in [0, T]$. Our numerical experiments have been performed on a sequence of refined meshes and for the polynomial degrees $p = 1, 2, 3, 4$ in the cases $d = 1$ as well as $d = 2$. In the case of smooth solutions, we have nicely observed the full asymptotical convergence rates. For simplicity, we restricted our-self to the single-patch case. However, it is possible to generalize the results to the conform multi-patch case. Moreover, the combination of the results of this paper with the results of the papers [33] and [39] allows us to analyze space-time multi-patch dG IgA schemes in a similar way. The overall efficiency of the space-time IgA heavily depends on the availability of fast parallel solvers. At the first glance, the solution of one large space-time system of linear algebraic equations instead of many smaller systems in traditional time-stepping methods seems to be

a big disadvantage of space-time IgA, but on parallel computers with many cores this is a big advantage that allows us to overcome the curse of sequentiality as Example 6.3 shows. Another advantage consists in the elegant treatment of moving domains or interfaces. And last, but not least the space-time adaptivity or, more precisely, the possibility to perform a free adaptivity in Q without separating the time from the space (t is just another variable x_{d+1}) opens new horizons in developing highly efficient parallel adaptive space-time IgA methods for parabolic as well as hyperbolic problems, using T-splines [45] or THB-splines [16] for local refinement.

Acknowledgment

The research is supported by the Austrian Science Fund (FWF) through the NFN S117-03 project. We also want to thank P. Vassilevski for the possibility to compute on the Vulcan Cluster in Livermore. Especially M. Neumüller wants to thank him for the support during his one month visit at the Lawrence Livermore National Laboratory.

References

1. R. Andreev. Stability of sparse space-time finite element discretizations of linear parabolic evolution equations. *IMA J. Numer. Anal.*, 33(1):242–260, 2013.
2. I. Babuška and T. Janik. The h - p version of the finite element method for parabolic equations. I. The p -version in time. *Numer. Methods Partial Differential Equations*, 5(4):363–399, 1989.
3. I. Babuška and T. Janik. The h - p version of the finite element method for parabolic equations. II. The h - p version in time. *Numer. Methods Partial Differential Equations*, 6(4):343–369, 1990.
4. F. Bachinger, U. Langer, and J. Schöberl. Numerical analysis of nonlinear multi-harmonic eddy current problems. *Numerische Mathematik*, 100:593–616, 2005.
5. R. Bank and P. Vassilevski. Space-time diskretization and solvers via time dependent embedding. privat communication.
6. R.E. Bank and M.S. Metti. An error analysis of some higher order space-time moving finite elements. *Comput Visual Sci*, 16:219–229, 2013.
7. Y. Bazilevs, L. Beirão da Veiga, J.A. Cottrell, T.J.R. Hughes, and G. Sangalli. Isogeometric analysis: Approximation, stability and error estimates for h -refined meshes. *Comput. Methods Appl. Mech. Engrg.*, 194:4135–4195, 2006.
8. M. Behr. Simplex space-time meshes in finite element simulations. *Internat. J. Numer. Methods Fluids*, 57:1421–1434, 2008.
9. N. Chegini and R. Stevenson. Adaptive wavelet schemes for parabolic problems: sparse matrices and numerical results. *SIAM J. Numer. Anal.*, 49(1):182–212, 2011.
10. J. A. Cottrell, T. J. R. Hughes, and Y. Bazilevs. *Isogeometric Analysis: Toward Integration of CAD and FEA*. John Wiley & Sons, Chichester, 2009.

11. A. Deshpande, S. Malhotra, M.H. Schultz, and C.C. Douglas. A rigorous analysis of time domain parallelism. *Parallel Algorithms and Applications*, 6(1):53–62, 1995.
12. John A. Evans and Thomas J.R. Hughes. Explicit trace inequalities for isogeometric analysis and parametric hexahedral finite elements. *Numerische Mathematik*, 123(2):259–290, 2013.
13. M. Gander. 50 years of time parallel time integration. In T. Carraro, M. Geiger, S. Körkel, and R. Rannacher, editors, *Multiple Shooting and Time Domain Decomposition*. Springer-Verlag, 2015. to appear.
14. M. J. Gander and M. Neumüller. Analysis of a new space-time parallel multigrid algorithm for parabolic problems. NuMa-Report 2014-08, Johannes Kepler University Linz, Institute for Computational Mathematics, Linz, November 2014.
15. M. J. Gander and M. Neumüller. Analysis of a time multigrid algorithm for DG-discretizations in time. NuMa-Report 2014-07, Johannes Kepler University Linz, Institute for Computational Mathematics, Linz, September 2014.
16. C. Giannelli, B. Jüttler, and H. Speleers. Thb-splines: The truncated basis for hierarchical splines. *Computer Aided Geometric Design*, 29(7):485–498, 2012.
17. W. Hackbusch. Parabolic multigrid methods. In R. Glowinski and J. L. Lions, editors, *Computing Methods in Applied Sciences and Engineering VI*, pages 189–197. North-Holland, Amsterdam, 1984.
18. P. Hansbo. Space-time oriented streamline diffusion methods for nonlinear conservation laws in one dimension. *Comm. Numer. Methods Engrg.*, 10(3):203–215, 1994.
19. G. Horton and S. Vandewalle. Fourier mode analysis of the multigrid waveform relaxation and time-parallel multigrid methods. *Computing*, 54:317–330, 1995.
20. T. J. R. Hughes, J. A. Cottrell, and Y. Bazilevs. Isogeometric analysis: CAD, finite elements, NURBS, exact geometry and mesh refinement. *Comput. Methods Appl. Mech. Engrg.*, 194:4135–4195, 2005.
21. C. Johnson. *Numerical solution of partial differential equations by the finite element method*. Dover Publications, Inc., Mineola, NY, 2009. Reprint of the 1987 edition.
22. C. Johnson, U. Nävert, and J. Pitkäranta. Finite element methods for linear hyperbolic problems. *Comput. Methods Appl. Mech. Engrg.*, 45(1-3):285–312, 1984.
23. C. Johnson and J. Saranen. Streamline diffusion methods for the incompressible Euler and Navier-Stokes equations. *Math. Comp.*, 47(175):1–18, 1986.
24. B. Jüttler, U. Langer, A. Mantzaflaris, S. E. Moore, and W. Zulehner. Geometry + Simulation Modules: Implementing Isogeometric Analysis. In P. Steinmann and G. Leugering, editors, *PAMM*, volume 14 of 1, pages 961–962, Erlangen, 2014.
25. E. Karabelas and M. Neumüller. Generating admissible space-time meshes for moving domains in $(d + 1)$ -dimensions. NuMa-Report 2015-07, Johannes Kepler University Linz, Institute for Computational Mathematics, Linz, November 2015.
26. P. Knabner and L. Angerman. *Numerical Methods for Elliptic and Parabolic Partial Differential Equations*, volume 44 of *Texts in Applied Mathematics*. Springer Verlag, New York, Berlin, Heidelberg, 2003.
27. M. Kollmann, M. Kolmbauer, U. Langer, M. Wolfmayr, and W. Zulehner. A finite element solver for a multiharmonic parabolic optimal control problem. *Computers and Mathematics with Applications*, 65:469–486, 2013.
28. M. Kolmbauer and U. Langer. A robust preconditioned-minres-solver for distributed time-periodic eddy current optimal control problems. *SIAM Journal on Scientific Computing*, 34(6):B785–B809, 2012.
29. O. A. Ladyzhenskaya. *The Boundary Value Problems of Mathematical Physics*. Nauka, Moscow, 1973. In Russian. Translated in *Appl. Math. Sci.* 49, Springer, 1985.

30. O. A. Ladyzhenskaya, V. A. Solonnikov, and N. N. Uraltseva. *Linear and Quasilinear Equations of Parabolic Type*. Nauka, Moscow, 1967. In Russian. Translated in AMS, Providence, RI, 1968.
31. J. Lang. *Adaptive Multilevel Solution of Nonlinear Parabolic PDE Systems. Theory, Algorithm, and Applications*, volume 16 of *Lecture Notes in Computational Sciences and Engineering*. Springer Verlag, Heidelberg, Berlin, 2000.
32. U. Langer, S. Repin, and M. Wolfmayr. Functional a posteriori error estimates for parabolic time-periodic boundary value problem. *Computational Methods in Applied Mathematics*, 15(3):353–372, 2015.
33. U. Langer and I. Touloupoulos. Analysis of discontinuous Galerkin IgA approximations to elliptic boundary value problems. NFN Technical Report 15, Johannes Kepler University, Linz, Geometry and Simulation, Linz, 2014.
34. C. Lehrenfeld. The Nitsche XFEM-DG Space-Time Method and its Implementation in Three Space Dimensions. *SIAM Journal on Scientific Computing*, 37(1):A245–A270, 2015.
35. J.-L. Lions, Y. Maday, and G. Turinici. A parareal in time discretization of PDEs. *C.R. Acad. Sci. Paris, Serie I*, 332:661–668, 2001.
36. C. Lubich and A. Ostermann. Multigrid dynamic iteration for parabolic equations. *BIT*, 27:216–234, 1987.
37. A. Masud and T.J.R. Hughes. A space-time Galerkin/least-squares finite element formulation of the Navier-Stokes equations for moving domain problems. *Comput. Methods Appl. Mech. Engrg.*, 146:91–126, 1997.
38. C. Mollet. Stability of petrov-galerkin discretizations: Application to the space-time weak formulation for parabolic evolution problems. *Computational Methods in Applied Mathematics*, 14(2):231–255, 2014.
39. M. Neumüller. *Space-Time Methods: Fast Solvers and Applications*, volume 20 of *Monographic Series TU Graz: Computation in Engineering and Science*. TU Graz, 2013.
40. M. Neumüller and O. Steinbach. Refinement of flexible space–time finite element meshes and discontinuous Galerkin methods. *Comput. Visual. Sci.*, 14:189–205, 2011.
41. M. Neumüller and O. Steinbach. A DG space–time domain decomposition method. In R. Bank, M. Holst, O. Widlund, and J. Xu, editors, *Domain Decomposition Methods in Science and Engineering XX*, pages 623–630, Berlin, Heidelberg, 2013. Springer.
42. M.A. Olshanskii and A. Reusken. Error analysis of a space-time finite element method for solving PDEs on evolving surfaces. *SIAM J. Numer. Anal.*, 2014.
43. M.A. Olshanskii, A. Reusken, and X. Xu. An Eulerian space-time finite element method for diffusion problems on evolving surfaces. *SIAM J. Numer. Anal.*, 52(3):1354–1377, 2014.
44. C. Schwab and R. Stevenson. Space–time adaptive wavelet methods for parabolic evolution problems. *Math. Comput.*, 78:1293–1318, 2009.
45. M.A. Scott, R.N. Simpson, J.A. Evans, S. Lipton, S.P.A. Bordas, T.J.R. Hughes, and T.W. Sederberg. Isogeometric boundary element analysis using unstructured T-splines. *Computer Methods in Applied Mechanics and Engineering*, 254:197–221, 2013.
46. O. Steinbach. Space-time finite element methods for parabolic problems. *Comput. Meth. Appl. Math.*, 15(4), 2015. to appear.
47. A. Tagliabue, L. Dedé, and A. Quarteroni. Isogeometric analysis and error estimates for high order partial differential equations in fluid dynamics. *Computers & Fluids*, 102:277 – 303, 2014.

48. T.E. Tezduyar. Interface-tracking and interface-capturing techniques for finite element computation of moving boundaries and interfaces. *Computer Methods in Applied Mechanics and Engineering*, 195(23):2983–3000, 2006.
49. T.E. Tezduyar, M. Behr, and J. Liou. A new strategy for finite element computations involving moving boundaries and interfaces—the deforming-spatial-domain/space-time procedure. I: The concept and the preliminary numerical tests. *Computer Methods in Applied Mechanics and Engineering*, 94(3):339–351, 1992.
50. T.E. Tezduyar, M. Behr, S. Mittal, and J. Liou. A new strategy for finite element computations involving moving boundaries and interfaces—the deforming-spatial-domain/space-time procedure: II. Computation of free-surface flows, two-liquid flows, and flows with drifting cylinders. *Computer Methods in Applied Mechanics and Engineering*, 94(3):353–371, 1992.
51. T.E. Tezduyar and S. Sathe. Enhanced-discretization space-time technique (ED-STT). *Comput. Methods Appl. Mech. Engrg.*, 193:1385–1401, 2004.
52. V. Thomée. *Galerkin Finite Element Methods for Parabolic Problems (Springer Series in Computational Mathematics)*. Springer-Verlag New York, Inc., Secaucus, NJ, USA, 2006.
53. F. Tröltzsch. *Optimal Control of Partial Differential Equations: Theory, Methods, and Applications*. Graduate studies in mathematics. American Mathematical Society, 2010.
54. K. Urban and A. T. Patera. An improved error bound for reduced basis approximation of linear parabolic problems. *Math. Comput.*, 83:1599–1615, 2014.
55. J. J. W. van der Vegt and H. van der Ven. Space-time discontinuous Galerkin finite element method with dynamic grid motion for inviscid compressible flows. I. General formulation. *J. Comput. Phys.*, 182:546–585, 2002.
56. S. Vandewalle. *Parallel Multigrid Waveform Relaxation for Parabolic Problems*. Teubner Skripten zur Numerik. Teubner, 1993.
57. J. Wloka. *Partielle Differentialgleichungen*. Teubner Verlag, Stuttgart, 1982. In German. Translated in *Cambridge University Press*, 1987.
58. S. Yamada and K. Bessho. Harmonic field calculation by the combination of finite element analysis and harmonic balance method. *IEEE Transactions on Magnetics*, 24(6):2588–2590, 1988.
59. E. Zeidler. *Nonlinear Functional Analysis and its Applications. II/A: Linear monotone operators*. Springer-Verlag, New York, 1990.